Combined Experimental and Computational Mechanistic Investigation of the Palladium Catalyzed Decarboxylative Cross-Coupling of Sodium Benzoates with Chloroarenes

Jenna N. Humke[1], Ryan A. Daley[1], Aaron S. Morrenzin[2], Sharon R. Neufeldt[2]*, Joseph J. Topczewski[1]*

[1]Department of Chemistry, University of Minnesota Twin Cities, Minneapolis, Minnesota 55455, United States

jtopczew@umn.edu

[2]Department of Chemistry and Biochemistry, Montana State University, Bozeman, Montana 59717, United States

sharon.neufeldt@montana.edu

KEYWORDS (Word Style "BG_Keywords"). palladium, cross-coupling, decarboxylation, mechanism, catalysis.

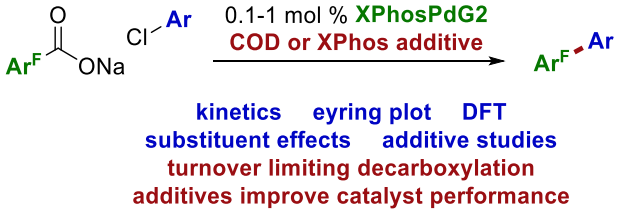

ABSTRACT: Reported herein is a mechanistic investigation into the palladium catalyzed decarboxylative cross-coupling of sodium benzoates and chloroarenes. The reaction was found to be first order in Pd. A minimal substituent effect was observed with respect to the chloroarene and the reaction was zero order with respect to chloroarene. Palladium mediated decarboxylation was assigned as the turn-over limiting step based on an Eyring plot and DFT computations. Catalyst performance was found to vary based on the electrophile, which is best explained by catalyst decomposition at Pd(0). The COD ligand contained in the precatalyst CODPd(CH_2TMS)$_2$ (**Pd1**) was shown to be a beneficial additive. The bench stable Buchwald complex **XPhosPdG2** could be used with exogenous COD and XPhos instead of complex **Pd1**. Adding exogenous XPhos significantly increased the catalyst TON and enhanced reproducibility.

■ Introduction

Cross-coupling reactions are used to synthesize pharmaceuticals, agrochemicals, and organic-electronics.[1,2] Unfortunately, the nucleophile (e.g. boronic acid) can be expensive, difficult to synthesize, or unstable under cross-coupling conditions.[3−6] In contrast, decarboxylative cross-coupling utilizes inexpensive, stable, and readily available carboxylates as the nucleophilic component.[7−17] However, even with recent progress, decarboxylative reactions frequently suffer from limitations including restricted substrate scope, elevated temperatures, high catalyst loadings, and the requirement for stoichiometric additives. This work has been summarized in several review articles, which provide more details about these transformations.[7−9,12,13,18−23]

The mechanisms of metal catalyzed protodecarboxylation and decarboxylative cross-coupling reactions have been studied.[10,11,24] In contrast to systems that use Ag[15,25−27] or Cu[21,25−32] additives, systems utilizing only a Pd catalyst are much less well understood. Unlike decarboxylative Heck reactions[33] or protodecarboxylation reactions,[34] there is minimal experimental mechanistic data on palladium catalyzed decarboxylative cross-coupling without copper or silver.[35−37] A variety of palladium catalyzed methods have been developed including work by Bilodeau and Forgione on coupling heteroarylcarboxylic acids,[35,38] a report by Eli Lilly to synthesize a desired scaffold,[39,40] and advancement of intramolecular cyclizations by Shen,[41,42] in addition to others.[43,44] However, these reactions have not been adequately investigated. Cross-coupling without stoichiometric additives is deceptively challenging due to halide inhibition.[33] A detailed mechanistic understanding is crucial to improve catalysis. More comprehensive data is needed to advance the field of palladium catalyzed decarboxylative cross-coupling reactions.

We reported the cross-coupling of sodium (hetero)aryl carboxylates with chloroarenes (Scheme 1).[45] Compared to prior work, this reaction i) uses inexpensive aryl chlorides, ii) displays an improved scope, iii) requires only 1.0 mol % Pd, iv) does not require any stoichiometric additives, and v) produces only NaCl and CO_2 as stoichiometric byproducts. However, several limitations to the reaction were noted, particularly with indole containing electrophiles. Furthermore, some irreproducibility was observed in coupling electron-rich aryl chlorides at reduced catalyst loadings.

Scheme 1. Reported Pd Catalyzed Decarboxylative Cross-Coupling

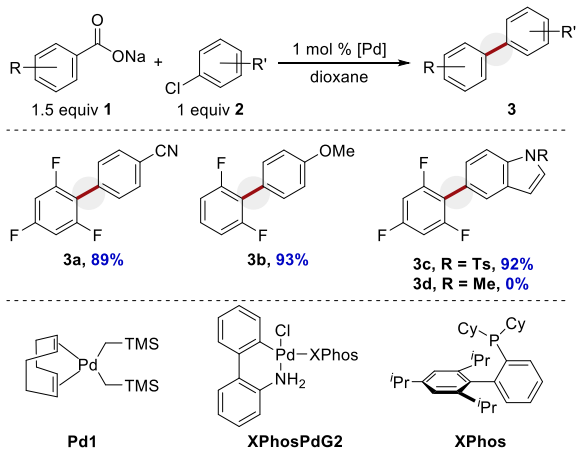

Based on computations by Liu,[36] the most probable mechanism involves pre-catalyst activation (Scheme 2, step i) followed by oxidative addition (step ii). Salt metathesis affords a Pd(II) carboxylate (step iii), which undergoes turn-over limiting decarboxylation (step iv). Reductive elimination affords product and regenerates the Pd(0) catalyst (step v).

While Liu's prior work is informative, there are several significant differences between the reaction Liu studied computationally and our optimized experimental conditions. These variations include i) using XPhos as the ligand, whereas prior calculations used PMe_3 as a model phosphine,[46] ii) using a sodium carboxylate instead of the potassium salt, and iii) using less activated benzoates, as opposed to pentafluorobenzoate. Additionally, experimental mechanistic studies on a palladium-catalyzed decarboxylative cross-coupling have not been previously provided in the absence of silver or copper.

Several preliminary observations further prompted this study. Substrate **2c**, featuring an *N*-Ts protected indole, afforded product **3c** in 92% yield (Scheme 1).[45] However, *N*-Me indole **2d** did not afford product **3d**. For most substrates, Buchwald precatalyst **XPhosPdG2**, which is commercially available and bench stable, provided similar results to the precatalyst CODPd($CH_2TMS)_2$ (**Pd1**), which is relatively expensive and is both temperature and air sensitive. However, for electron-rich aryl-chlorides (such as 4-chloroanisole, **2b**), precatalyst **Pd1** was superior. These issues are not explained by the proposed mechanism (Scheme 2). Furthermore, some irreproducibility was observed with electron-rich substrates. These observations, along with a substrate dependence on the reaction time course kinetic profile (*vide infra*), prompted a more detailed mechanistic study, the results of which are reported herein.

Scheme 2. Liu's Mechanism for Decarboxylative Cross-Coupling Based on DFT

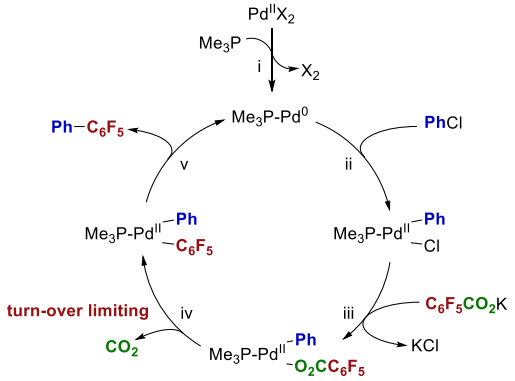

■ RESULTS AND DISCUSSION

Kinetic Order in Palladium and Ligands. Based on the original optimization,[45] two different catalyst systems could be utilized: i) 1 mol % **XPhosPdG2** or ii) a combination of 1 mol % **Pd1** and 2 mol % XPhos.[45] Initial kinetic studies used **XPhosPdG2** because it contains a predetermined 1:1 Pd to XPhos ratio and has enhanced bench stabilty.[47,48] The kinetic order in [Pd] was determined for the coupling of carboxylate **1a** and chloride **2a** (Figure 1). Based on the method of initial rates[49] the reaction was first order in **XPhosPdG2** (k_{obs} = 1.61 x 10^{-6} with 2.0 μM [Pd], 1 mol % Pd) (Figure 1). This is consistent with a monomeric palladium complex being involved in the turn-over limiting step.

Figure 1. Order in Catalyst

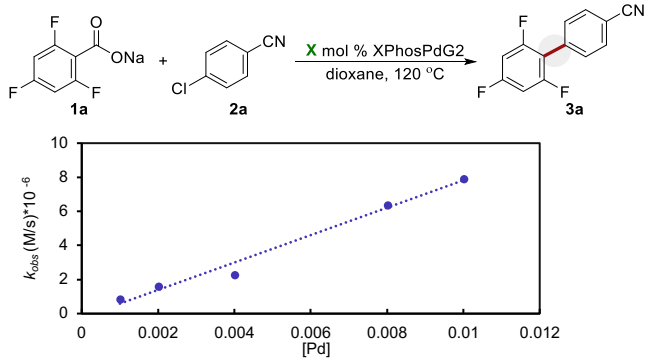

k_{obs} calculated based on the method of initial rates with product [**3a**] measured via calibrated GC-FID. Each point reflects the average of duplicate trials at a given Pd loading. Reactions conducted with benzoate **1a** (0.15 mmol), chloroarene **2a** (0.10 mmol), in dioxane (0.2 M), with 0.5 – 5.0 mol % **XPhosPdG2** (plotted in units of *M*), Dashed line represents a least squares linear regression with R^2 = 0.98.

Inverse order with respect to ligand is common for palladium-catalyzed systems when ligand dissociation is required prior to oxidative addition.[50,51] Buchwald style ligands are known to favor an LPd(0) complex instead of an $L_nPd(0)$ complex (n = 2-4).[48,52–59] Carbazole can inhibit some palladium catalyzed couplings,[60–63] This reaction was found to be near zeroth order with respect to added XPhos, carbazole, and carbazole HCl (see SI). These data indicate that the advantage of precatalyst **Pd1**/XPhos, over **XPhosPdG2**, cannot be ascribed to by-product formation upon **XPhosPdG2** activation. Lastly, XPhos oxide was not observed at the end of the reaction by ^{31}P NMR (see SI), indicating that the excess XPhos used with **Pd1** (2 mol % instead of 1 mol % in **XPhosPdG2**) was not merely functioning for precatalyst activation or as a sponge for adventitious oxygen.[64–66] These observations prompted an investigation into the oxidative addition step.

Oxidative Addition. The reaction time course profile was observed to differ significantly depending on the chloroarene (Figure 2). With substrate **2a** (R = CN), product formation was linear with respect to time throughout the reaction (apparent zeroth order, Figure 2a). This kinetic profile would be expected for a catalytic reaction with a single slow step and no product inhibition ([S] + [cat] → [P] + [cat] with the rate only dependent on [cat] when saturated in [S]). In contrast, with substrate **2b** (R = OMe, Figure 2b), the time course showed a stark curvature and failed to reach complete conversion with 1 mol % **PdXPhosG2**. This observation suggests that the nature of the electrophile influences the overall reaction profile and triggered an exploration into the oxidative addition step.

Figure 2. Full Reaction Time Course

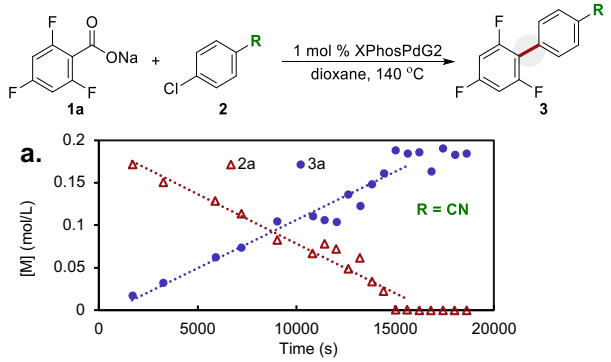

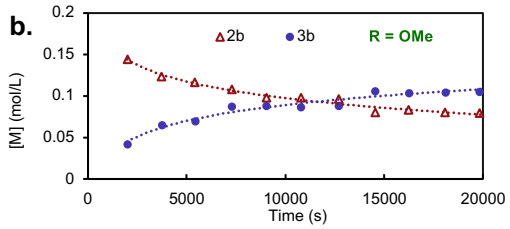

a. R = CN, lines represent a linear fit for reaction progression. **b.** R = OMe, lines represent a logarithmic fit for reaction progression. Substrate [**2**] and product [**3**] were measured via calibrated GC-FID. Reactions conducted with benzoate **1a** (0.15 mmol), chloroarene (0.10 mmol), in dioxane (0.2 M), with 1 mol % **XPhosPdG2**.

For Pd(0), oxidative addition is well established to be faster with electron deficient haloarenes.[50] A series of competition experiments were conducted under saturating conditions (Table 1, 10 equiv of each chloroarene). With 4-chlorobenzonitrile (σ_p = 0.66), the 4-benzonitrile product (**3a**) always predominated (Table 1, entries 1-3). With 4-chloroanisole (σ_p = -0.27) vs chlorobenzene (σ_p = 0, entry 4) or vs 4-*tert*-butyl-chlorobenzene (σ_p = -0.2, entry 5), a mixture of products was observed. This significant substituent effect is consistent with prior work with Pd oxidative addition and is consistent with the varied kinetic profile shown in Figure 2. However, the initial rate was found to be near zeroth order with respect to aryl chloride (4-chlorobenzonitrile, **2a**, see SI). A Hammett plot was constructed using the method of initial rates[49] (Figure 3). Across the traditional Hammett series, the ρ value was small (ρ = 0.15, k_{rel} 4-CN/4-OMe ~2, OMe σ_p = -0.27, CN σ_p = 0.66). This is consistent with Liu's mechanism where decarboxylation, not oxidative addition, is turnover limiting (Scheme 2). These data support the conclusions that i) the rate of this elementary step does vary based on the substrate, and ii) oxidative addition is not turn-over limiting under catalytic conditions. This is sensible based on the reported rate of isolated oxidative addition reactions.[50] The observed difference in the reactivity profile (Figure 2) may indicate that varying the arene may influence other steps of the catalytic cycle, potentially decarboxylation or the catalyst resting state (*vide infra*).

Table 1. Competition Experiment

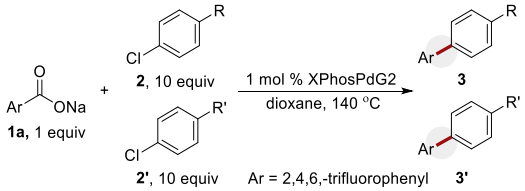

Entry	R = , σ_p	R' = , σ_p	**3** (%)	**3'** (%)	**3:3'**
1	CN, 0.66	H, 0	92	<5	nc
2	CN, 0.66	^{t}Bu, -0.2	90	n.d.	nc
3	CN, 0.66	OMe, -0,27	>95	<5	nc
4	H, 0	OMe, -0.27	59	30	2.0:1
5	^{t}Bu, -0.2	OMe, -0.27	51	34	1.5:1

Reactions conducted with benzoate **1a** (0.10 mmol), chloroarenes (1.0 mmol each), in dioxane (0.17 M), with 1 mol % **XPhosPdG2**. Yields determined by calibrated GC-FID. All yields reflect the average of duplicate trials. n.d. = not detected, nc = not calculated.

Figure 3. Hammett Plot

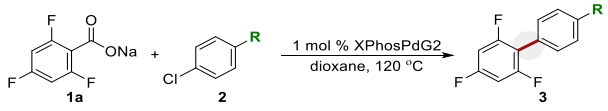

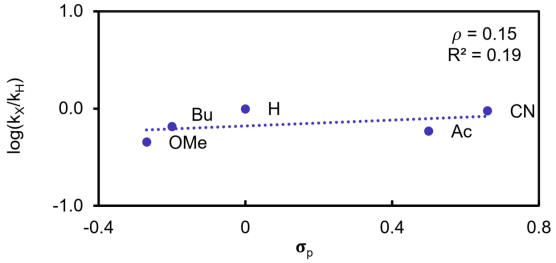

Values for k_{obs} calculated based on the method of initial rates with product [**3**] measured via calibrated GC-FID. Each point reflects the average of duplicate trials with a given chloroarene. Reactions conducted with benzoate **1a** (0.15 mmol), chloroarene (0.10 mmol), in dioxane (0.2 M), with 1 mol % **XPhosPdG2.**

Decarboxylation. Based on the data presented, oxidative addition does not appear turn-over limiting, making decarboxylation the likely turn-over limiting step. The reaction was observed to exhibit zero order dependence on carboxylate **1a**, which is likely due to the insolubility of the sodium carboxylate in the reaction media. To investigate the activation barriers for the catalytic cycle, the initial rate was measured at different temperatures with substrates **1a** and **2a** to construct an Eyring Plot (Figure 4).[67] Based on the slope and intercept, the activation barriers were calculated ($\Delta G^{\ddagger}$ = 33.9 kcal/mol, $\Delta H^{\ddagger}$ = 28.2 kcal/mol and $\Delta S^{\ddagger}$ = -14.0 cal/(mol*K)). Because decarboxylation is difficult to examine experimentally, a series of DFT calculations were conducted.

Liu's calculated catalytic cycle used the simplified model ligand PMe_3,[36] which varies significantly from the Buchwald-style ligands used in our optimized catalytic reaction. The experimentally optimized ligand is XPhos (2-dicyclohexylphosphino-2′,4′,6′-triisopropylbiphenyl). The catalytic cycle was calculated using SPhos (2-dicyclohexylphosphino-2',6'-dimethoxybiphenyl, shown in IN0) because SPhos is less conformationally flexible than XPhos, which streamlines the calculations. Based on our initial report, SPhos is an effective ligand experimentally[68] and it is structurally similar to XPhos. Density functional theory (DFT) calculations were performed with Gaussian16.[69] Geometry optimizations were conducted in the gas phase using the M06L functional. Energies were further refined with M06 using a larger basis set and 1,4-dioxane as implicit solvent (see Computational Methods and SI).[70]

Figure 4. Eyring Plot

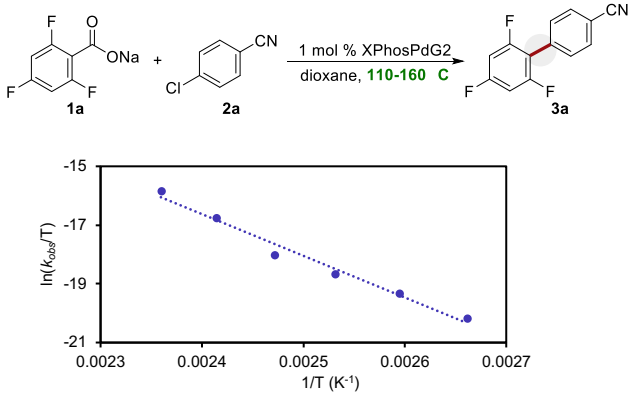

k_{Obs} calculated based on the method of initial rates with [**3a**] measured via calibrated GC-FID. Each point reflects the average of duplicate trials at a given temperature. Reactions conducted with benzoate **1a** (0.15 mmol), chloroarene (0.10 mmol), in dioxane (0.2 M), with 1 mol % **XPhosPdG2**.

Consistent with the literature,[36] calculations on the cross-coupling of substrates **1a** with **2b** (Figure 1) indicate that decarboxylation is the turn-over limiting step. The calculated energy span for decarboxylation (**TS2-a**) is 31.7 kcal/mol when measured from the lowest preceding intermediate (**IN2**). Compared to the previously calculated barrier using pentafluorobenzoate and PMe_3 as a model phosphine (24.0 kcal/mol),[36] this calculated barrier is more in line with the experimentally obtained free energy of activation for our system (33.9 kcal/mol, Figure 4). Oxidative addition (**TS1**) is predicted to be much faster than decarboxylation, with a free energy barrier of only 15.7 kcal/mol measured from the preceding complex **IN1** for 4-chloroanisole. This trend remains consistent for all calculated (hetero)aryl chloride/carboxylate combinations (see SI). Notably, oxidative addition of an electron-deficient aryl chloride is predicted to be faster (12.7 kcal/mol for 4-chlorobenzaldehyde vs. 15.7 kcal/mol for 4-chloroanisole),

which is consistent with the competition experiments in Table 1 (see SI for full details).

Another difference between the mechanism calculated here and the literature is the relative stability of the palladium(II) carboxylate (**IN3-a**). These calculations indicate that salt metathesis is endergonic (ΔG=+13.5 kcal/mol), whereas prior calculations using PMe_3 predicted an exergonic salt metathesis. This discrepancy likely relates to ligand structure. SPhos is hemilabile, making **IN2** a 16-electron complex. When chloride is exchanged, the distal arene in SPhos must dissociate to accommodate the κ^2-carboxylate (**IN3-a**). In contrast, the PMe_3-containing analog to **IN2** reported in the prior calculations is a 14-electron complex, which is stabilized by forming a 16-electron κ^2-carboxylate product via salt metathesis. The use of different counter cations (K vs. Na) may also contribute to energy differences between the two sets of calculations. However, it is worth noting that error in the calculated energies may arise from our use of an implicit solvent model, which cannot fully capture the effects of solvent coordination to ionic species.

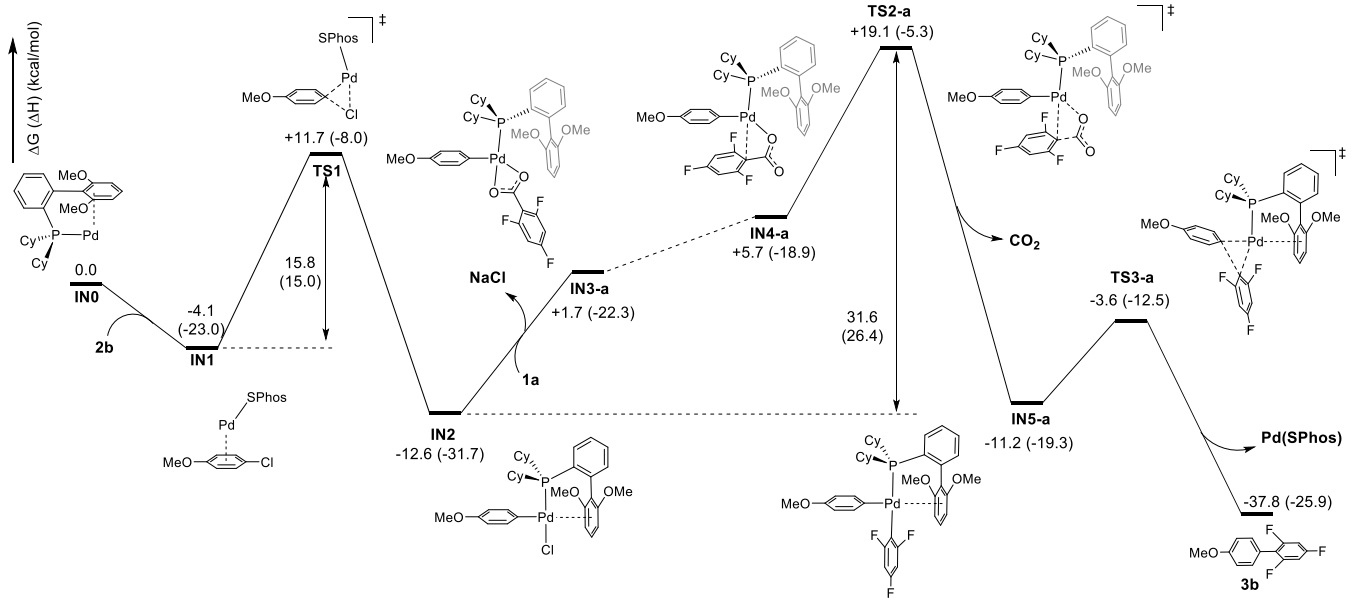

Figure 5. Calculated free energy reaction coordinate diagram for the decarboxylative cross-coupling of 4-chloroanisole with 2,4,6-trifluorobenzoate

Table 2. Calculated Free Energies of Activation for Decarboxylation

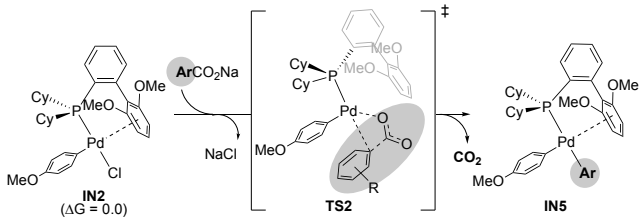

Entry	Ar	TS2[a] ΔG‡ (kcal/mol)	IN5[a] ΔG (kcal/mol)
1	3,4,5-trifluorophenyl	**TS2-f**, 41.2	11.5
2	4-fluorophenyl	**TS2-d**, 41.3	8.8
3	phenyl	**TS2-b** ,40.8	12.3
4	2-fluorophenyl	**TS2-e**, 36.1	6.6
5	2,4,6-trifluorophenyl	**TS2-a**, 31.6	1.4
6	2,6-dimethoxyphenyl	**TS2-c**, 26.7	–3.9

Free energy values are measured relative to **IN2**, whose energy is defined as 0.0 kcal/mol for this comparison.

Hoover and coworkers recently reported that the field effect parameter has good predictive power for the rate of decarboxylation of silver benzoates.[15] Inspired by this work, DFT was used to compare the barriers for decarboxylation of several substituted benzoates at Pd. These calculations were conducted using coupling partner **2b** (i.e., using a 4-methoxyphenyl palladium complex, Table 2). Activation free energies were measured from the lowest energy intermediate (**IN2**) that precedes the decarboxylation transition structure. Substrates containing *ortho* fluorines or oxygens are calculated to have the smallest barriers to decarboxylation. For example, the activation barrier using 2,4,6-trifluorobenzoate is only 30.3 kcal/mol compared to a barrier of 40.9 kcal/mol with 3,4,5-trifluorobenzoate. This finding is consistent with a field effect correlation. Analysis of the electrostatic potential surfaces for the decarboxylation transition structures also reveals features expected based on field effects. In particular, electronegative *ortho* substituents provide regions of negative electrostatic potential in close proximity to the negative carboxylate (Figure 6). This phenomenon is indicative of electron repulsion, which may serve as a driving force for expulsion of CO_2. It should be noted that the relative rankings of entries 5 and 6 in Table 2 are not fully consistent with the field effect parameter (flourine has a larger field effect parameter then methoxy). In this respect, Pd mediated decarboxylation may not have as strong of a correlation to the field effect parameter as the decarboxylation of Ag carboxylates.[15] Ag and Pd mediated decarboxylation have been shown to exhibit different substrate dependences, so different effects, such as arene acidity, may contribute to the relative ease of decarboxylation.[71]

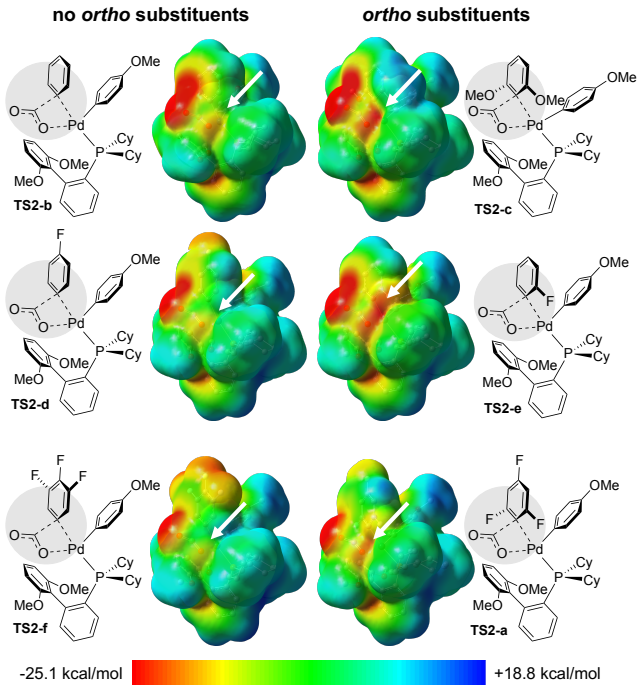

Figure 6. Electrostatic potential maps of decarboxylation transition structures

Chloroindoles. Attention turned to investigating the substrate limitations of the catalytic cross-coupling. Heterocycles are common motifs in pharmaceuticals,[72,73] but tend to be challenging substrates for cross-coupling.[74,75] The reaction with 5-chloro-1-tosyl indole (**2c**) afforded a 92% yield; however, 5-chloro-1-methyl indole (**2d**) afforded only trace product (Scheme 1). To determine if the indole acts as a catalyst poison [74,76–78] substrates **1a** and **2a** were utilized in the presence or absence of added indole to conduct an additive screen.[79,80] Cross-coupling quantitatively affords biaryl **3a** (Table 3, entry 1). Adding a full equivalent of indole (entry 2) or *N*-methyl indole (entry 3) resulted in only a small yield reduction, indicating that these two indoles are not potent catalyst poisons. However, adding 5-chloro-1-methyl indole (entry 4) or 5-chloro indole (entry 5), resulted in a significantly diminished yield. The decrease in yield is not likely attributable to competitive cross-coupling of the comparatively electron rich chloro-indole (vis-à-vis Table 1). In the case of 5-chloroindole, the additive was consumed in the reaction. The complex mixture obtained may comprise products from a variety of possible side reactions, including homocoupling, C-H activation,[81–84] and catalyst decomposition. With 5-chloroindole, the desired cross-coupling was partially restored by increasing the catalyst loading to 20 mol % (entry 5, 78% yield in parenthesis), indicating that the issue is catalyst poisoning and not selectivity. As such, this result suggests that higher catalyst loadings may enable cross-coupling of challenging substrates.

Table 3. Indole Additive Screens

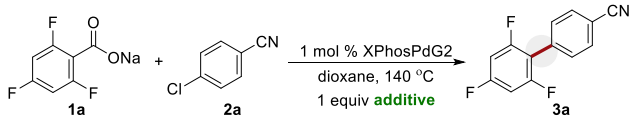

Entry[a]	Additive	% **2a**	% **3a**	% Additive
1	none	n.d.	>99	N/A
2		n.d.	78	68
3		n.d.	88	98
4	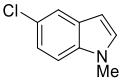	58	21	97
5	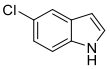	<5	34 (78[a])	33 (n.d.)

Reactions conducted with benzoate **1a** (0.15 mmol), chloroarene (0.10 mmol), additive (0.1 mmol) in dioxane (0.2 M), with 1 mol % **XPhosPdG2**. Yields determined by calibrated GC-FID. All yields reflect the average of duplicate trials. [a]Reaction conducted at 20 mol % catalyst loading. N/A = not applicable. n.d. = not detected.

A variety of chloroindoles were subjected to the reaction conditions with varied Pd loadings (Table 4). As originally noted, Indole **2c** works exceptionally well (Table 4, entry 1). Indoles with electron withdrawing groups afforded good yields (entries 2 - 3). The yield of *N*-methylindole **3d** improved with increased catalyst loading (entry 4). Some *N*H-indoles remain problematic even at higher Pd concentrations (**2e** and **2h**). However, 7-chloro-indole (**2i**) and 4-chloro-indole (**2j**) give good yields of product with 10 mol % Pd. The results in Table 4 did not correlate with the calculated barriers to oxidative addition (see SI). The origin of these varied results is not clear and warrants further investigation. Using additional XPhos and COD (*vide infra*) failed to further increase the yield of product **3d** (see SI).

Effect of COD and XPhos. Ideally, **XPhosPdG2** could be used with all substrates. Irreproducibility and poor conversion were noted (Figure 2, **2b**). With 0.1 mol % **Pd1** and 0.2 mol % XPhos, an 80% yield of product **3b** was observed.[45] The yield was only 24% with 0.1 mol % **XPhosPdG2**. Adding exogenous ligand with Buchwald ligands can improve yields.[59,85] It is possible that either COD or XPhos could be stabilizing the catalyst. When using **XPhosPdG2**, the initial rate was zero order in COD (See SI). As such, COD does not accelerate or inhibit decarboxylation. When COD was added to the cross-coupling of 4-chloroanisole with **XPhosPdG2**, the yield significantly improved at a 4h reaction time (Figure 7). With 1.0 mol % Pd, the reaction without COD had a 36% yield at 4h (blue circles), while the reaction with added COD afforded an 80% yield (red triangles). The yield varied in a sporadic manner with respect to catalyst loading at 4 h. If the primary catalyst decomposition pathway involves aggregation of Pd(0), which is commonly observed with palladium catalyzed transformations,[77,86–89] then at higher [Pd], catalyst decomposition would be faster and the reaction yield would be non-linear with respect to catalyst loading.

Table 4. Cross-Coupling with Various Chloroindoles

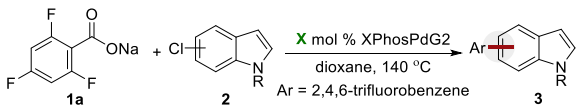

Entry	Substrate	% **3**[a]	% **3**[b]	% **3**[c]
1	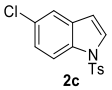 **2c**	97	-	-
2	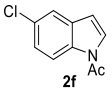 **2f**	53	90	90
3	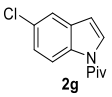 **2g**	44	46	47
4	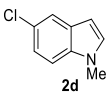 **2d**	n.d.	20	34
5	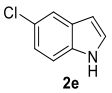 **2e**	<5	<5	8
6	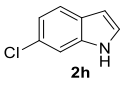 **2h**	n.d.	8	9

7	 2i	5	63	60
8	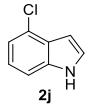 2j	8	64	67

Reactions conducted with benzoate **1a** (0.15 mmol), chloroarene (0.10 mmol), additive (0.1 mmol) in dioxane (0.2 M), with 1 - 20 mol % **XPhosPdG2**. Yields determined by ^{19}F NMR analysis. All yields reflect the average of duplicate trials, n.d. = not detected. [a] 1 mol % Pd, [b] 10 mol % Pd, [c] 20 mol % Pd.

The reaction time course profile changed when COD was added (Figure 8). With 0 mol % COD, the reaction rate clearly decreases over time. With 3 mol % added COD (see SI for additional data from 1-5 mol% COD), the reaction reached high conversion and the data closely resembled that with substrate **2a** (Figure 2a). As such, adding COD appears to be a viable strategy to improve catalyst performance with substrate **2b**. It should be noted that utilizing an alkene ligand, such as dba, to stabilize Pd(0) has been reported.[90–92] The reaction time course with both XPhos and COD (3 mol % of each) provided a similar result (Figure 8). These data suggest that catalyst death occurs from the aggregation of Pd(0), which can be slowed with COD and XPhos. The substrate dependence on oxidative addition (Table 1) and catalyst decomposition at Pd(0) would explain the observed difference in reaction progression for substrates **2a** and **2b** (Figure 2).

Figure 7. Effect of COD on Yield

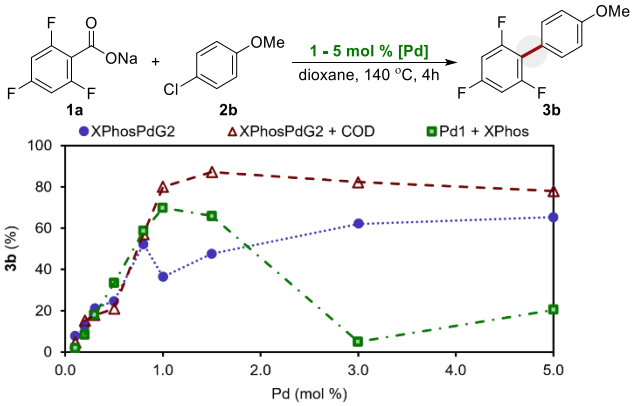

Reactions conducted with benzoate **1a** (0.15 mmol), chloroarene **2b** (0.10 mmol), in dioxane (0.2 M), with 0.1 – 5 mol **XPhosPdG2** (blue), 0.1 – 5 mol % *XPhosPdG2*/0.1 – 5 mol % COD (red), or 1 – 5 mol % Pd1/1 – 5 mol % XPhos. Yields determined by calibrated GC-FID. Each point represents the result of duplicate trials.

Figure 8. Full Time Course with Additional COD/XPhos

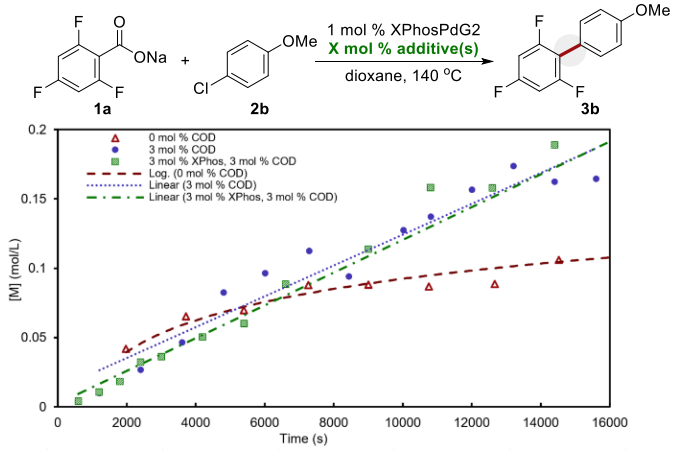

Reactions conducted with benzoate **1a** (0.15 mmol), chloroarene **2b** (0.10 mmol), in dioxane (0.2 M), with 1 mol % **XPhosPdG2** and 3 mol % additive(s). Concentrations determined by calibrated GC-FID. 0 mol % COD (red triangle) fit with a logarithmic curve (long dash,), 3 mol % COD (blue circle) and 3 mol % COD/3 mol % XPhos (green box) fit with a linear trend line (blue dot and green dot-dash, respectively).

Having observed a beneficial role of COD in the reaction, other additives were screened with the intent of increasing the catalyst turn-over number (Table 5 and SI). With no additive and 0.1 mol % **XPhosPdG2** the reaction had a TON of 235 (entry 1). The addition of 0.3 mol % COD or norbornadiene(NBD) was not as beneficial as adding 3 mol% (entries 2-3). When XPhos was added (entry 4), the TON increased dramatically to 820. This is comparable with the best TON originally observed with **Pd1** (800).[36] As such, the addition of XPhos and COD enables the use of the air stable complex **XPhosPdG2** instead of the more expensive and more sensitive precatalyst **Pd1**.

Revised Mechanism. The data reported support revision of the previously proposed mechanism (Scheme 3).[36] Decarboxylation is turn-over limiting as originally proposed and highly influenced by the nature of the ortho substituent. Catalyst death appears to result primarily from aggregation of Pd(0). Competition experiments and computations indicate that the rate of the elementary oxidative addition step is substrate dependent. When oxidative addition is relatively slow (substrate **2b**), palladium aggregation can occur, which results in catalyst death (Scheme 9, step vii). This explains the substrate dependent time course data (Figure 2). Catalyst death can be mitigated by the use of COD and XPhos as additives (Figures 7 and 8). The observation that COD and/or XPhos addition can improve catalyst performance may have implications to other palladium catalyzed systems.

Table 5. Effect of Additives on Turnover Number

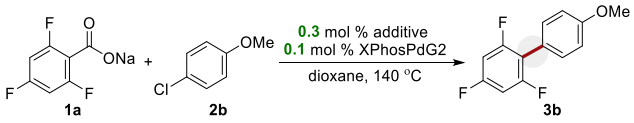

Entry	Additive	% **3b**	TON
1	none	24	235
2	COD	14	139
3	XPhos	82	822
4	NBD	18	188

Reactions conducted with benzoate **1a** (0.30 mmol), chloroarene **2b** (0.20 mmol), in dioxane (0.2 M), with 0.1 mol % **XPhosPdG2** and 0.3 mol % additive at 140 °C for 120 h. Yields determined by calibrated GC-FID. All yields reflect the average of 2-4 trials. NBD = norbornadiene

■ CONCLUSION

The mechanism of the palladium catalyzed decarboxylative cross-coupling of chloroarenes was investigated both experimentally and computationally. The reaction was found to be first order in palladium and zero-order in aryl chloride. DFT calculations and an Eyring analysis support decarboxylation as the turn-over limiting step. The substrate dependent behavior was found to be the result of catalyst decomposition at Pd(0). The addition of either COD or XPhos was found to improve the catalyst performance. With the addition of XPhos, bench stable precatalyst **XPhosPdG2** could replicate the best results obtained with complex **Pd1**. As such, the addition of either COD or XPhos is a promising development to decrease the catalyst loading and to expand the substrate scope of palladium catalyzed decarboxylative cross-coupling.

Scheme 3. Revised Mechanism

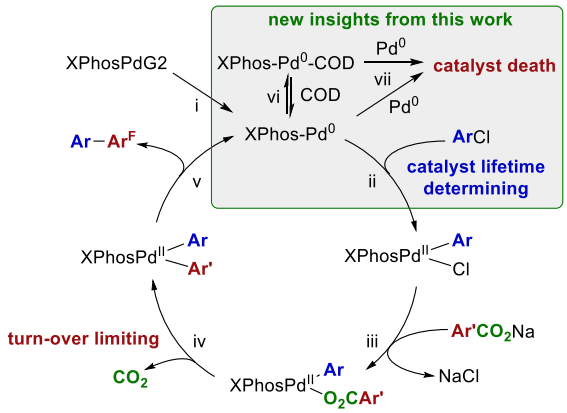

■ Experimental Section

General Notes for All Kinetic Trials: Following general procedures for kinetic trials, the vials were heated to the specified temperature. At the desired time point, the reactions were quenched by submerging the vial into an ice bath and the time was rounded to the nearest second. The reaction was diluted with DCM (ca. 2 mL). An aliquot of the reaction mixture was filtered through a short plug of silica gel and the silica gel was washed with DCM (2 mL). The filtrate was collected and analyzed by GC-FID. Concentrations and yields were determined by GC analysis of the reaction mixture using a linear regression based on a 5-point calibration curve with biphenyl as the internal standard. The rate of the reaction (k_{obs}) was determined by the method of initial rates. The initial rate under each set of reaction conditions was obtained by plotting the concentration of the product versus reaction time. The data was fit to a linear function using Excel. The slope of the fit was recorded as the initial rate of the reaction (M/s). Error in the fit was determined by the LINEST function in Excel. The rate calculated is reported in the SI along with the error. Each observed rate was determined in duplicate or triplicate. The replicate data is reported in the SI.

***General Procedure A for Kinetic Trials (XPhosPdG2)*: Preparation of [Pd] vials:** Example given for 1 mol % Pd. A 20 mL vial was charged with XPhosPdG2 (40.0 mg, 0.05 mmol) and dry DCM (20 mL) to prepare a [Pd] stock solution. An aliquot of the [Pd] stock solution (0.4 mL, 1.0 µmol [Pd]) was added to separate 4 mL vials. The vials were placed in a fume hood to evaporate the DCM under air. After 12-18 h, the vials were brought inside a glovebox and stored under a N_2 atmosphere for up to two weeks. **NOTE:** It was discovered that vials of [Pd] prepared in this manner could be used with little change in catalyst performance for up to 2 weeks. Using vials that were stored for more than 2 weeks resulted in less reproducible results (presumed catalyst decomposition).

Decarboxylative Cross-Coupling Reactions for Kinetic Experiments: A stock solution was prepared in a glovebox. A 20 mL vial was charged with aryl chloride **2a** (264.1 mg, 1.920 mmol), biphenyl (74.1 mg, 0.481 mmol, internal standard) and dioxane (9.5 mL). Separate vials containing [Pd] catalysts (as described above) were charged with benzoate **1a** (29.5-33.0 mg, ca.150 µmol) and an aliquot of the 4-chlorobenzonitrile solution (0.5 mL, 100 µmol). The vials were sealed with a Teflon-lined cap and removed from the glovebox.

General Procedure B for Kinetic Trials (Pd1): In a glovebox, a 20 mL vial was charged with CODPd(CH_2TMS)$_2$ (**Pd1**, 5.8 mg, 15 µmol) and dioxane (3.75 mL) to prepare a palladium stock solution. A 20 mL vial was charged with aryl chloride **2a** (207 mg, 1.50 mmol), biphenyl (60.7 mg, 399 µmol, internal standard) and dioxane (3.75 mL). Separate 4 mL vials were charged with benzoate **1a** (29.3-30.7 mg, ca. 150 µmol), an aliquot of the Pd stock solution (0.25 mL, ca. 1 mol % **Pd1**) and an aliquot of the **2a** solution (0.25 mL, ca. 100 µmol 2a). The vials were sealed with a Teflon-lined cap and removed from the glovebox.

Kinetic Order in XPhos (See SI): The kinetic order in XPhos was determined by studying the initial rate of reaction with different concentrations of XPhos from (0.002 - 0.02 M). General procedure B for kinetic trials was followed with minor modifications. Example given for XPhos = 5 mol % (0.01 M). Prior to general procedure B, XPhos vials were prepared. A 20 mL vial was charged with XPhos (35.9 mg, 75.3 µmol) and DCM (15 mL) and stirred for 1 h to prepare a XPhos stock solution. An aliquot of the XPhos stock solution (1.0 mL, 5.0 µmol XPhos) was added to separate 4 mL vials. The vials were placed in a fume hood to evaporate the DCM under air. After 18 h, the vials were brought inside a glovebox and stored under a N_2 atmosphere.

Kinetic Order in Carbazole (See SI): The kinetic order in carbazole was determined by studying the initial rate of reaction with different concentrations of carbazole from 0.004-0.02 M. General procedure B for kinetic trials was followed with minor modifications. Example given for carbazole = 5 mol % (0.01 M). Prior to general procedure B, XPhos/carbazole vials were prepared. A 20 mL vial was charged with XPhos (14.2 mg, 29.8 µmol), carbazole (12.5 mg, 74.8 µmol), and DCM (12 mL) and stirred for 1 h to prepare a XPhos/carbazole stock solution. An aliquot of the XPhos/carbazole stock solution (0.8 mL, 5.0 µmol carbazole, 2.0 µmol XPhos) was added to separate 4 mL vials. The vials were placed in a fume hood to evaporate the DCM under air. After 18 h, the vials were brought inside a glovebox and stored under a N_2 atmosphere.

Kinetic Order in Carbazole HCl (See SI): The kinetic order in carbazole·HCl was determined by studying the initial rate of reaction with different concentrations of carbazole·HCl from 0.004-0.02 M. Example given for 5 mol % carbazole·HCl. XPhos vials (2 mol % XPhos) were prepared as outlined in kinetic order in XPhos procedure. In a glovebox, a 4 mL vial was charged with **Pd1** (3.0 mg, 7.7 µmol) and dioxane (0.8 mL) to prepare a palladium stock solution. A separate 4 mL vial was charged with carbazole·HCl (8.3 mg, 41 µmol) and dioxane (1.2 mL) to prepare a carbazole·HCl stock solution. A 20 mL vial was charged with aryl chloride **2a** (207 mg, 1.50 mmol), biphenyl (57.9 mg, 380 µmol, internal standard) and dioxane (3.75 mL). Separate vials 4 mL vials were charged with **la** (29.9-32.5 mg, ca. 150 µmol), an aliquot of the Pd stock solution (0.25 mL, ca. 1 mol % **Pd1**), an aliquot of the **2a** solution (0.25 mL, ca. 0.100 µmol 2a), and an aliquot of the carbazole·HCl solution (0.15 mL, ca. 5.0 µmol). The vials were sealed with a Teflon-lined cap and removed from the glovebox.

Kinetic Order in XPhosPdG2 (Scheme 3): The kinetic order in palladium catalyst was determined by studying the initial rate of reaction with different concentrations of palladium from 0.001-0.010 M (0.5 mol % - 5.0 mol %). General procedure A for kinetic trials was followed.

General Procedure for Competition Experiments (Table 1): Example given for experiment between 4-chlorobenzonitrile(**2a**) and 4-chloroanisole(**2b**). A stock solution was prepared in a glovebox. A 20 mL vial was charged with **2a** (481.5 mg, 3.500 mmol), **2b** (499.1 mg, 3.500 mmol), biphenyl (13.7 mg, 0.0889 mmol, internal standard) and dioxane (1.75 mL). Separate vials containing [Pd] catalysts (as described above) in general procedure A were charged with sodium **1a** (19.8 mg, ca.100 µmol) and an aliquot of the aryl chloride solution (0.6 mL, 100 µmol). **NOTE:** When preparing the aryl chloride stock solution, the aryl chloride was used in large enough quantities to significantly change the total volume of the solution, therefore the volume of the aliquot taken was adjusted accordingly. The vials were sealed with a Teflon-lined cap and removed from the glovebox. The vials were heated to 140 °C. After 24 hours, the reactions were cooled to room temperature. The reaction was diluted with DCM (ca. 2 mL). An aliquot of the reaction mixture was filtered through a short plug of silica gel and the silica gel was washed with DCM (2 mL). The filtrate was collected and analyzed by GC-FID. The reactions were run in duplicate or triplicate and the average yield value was reported. **NOTE:** The competition experiment between 4-chloroanisole (**3a**) and chlorobenzene was conducted following the general procedure for competition experiments with minor modifications. Biphenyl (internal standard) was directly weighed into the [Pd] vials.

Hammett Plot (Scheme 5): The Hammett plot was constructed for the reaction of various aryl chloride substrates. General procedure A for kinetic trials was followed.

Kinetic Order in ArCl (See SI): The kinetic order in aryl chloride was determined by studying the initial rate of reaction with different concentrations of aryl chloride from 0.025-0.15 M. The reactions were conducted following the general procedure A for kinetic data with the following minor modifications. To maintain pseudo-first-order conditions, the benzoate **1a** substrate was used in excess (59.4 mg, 0.3 mmol). For solubility reasons, the reactions were run twice as dilute in dioxane (1 mL, 0.3 M with respect to **1a**).

Eyring Plot (Scheme 6): The temperature was varied (100 – 160 °C). General procedure A for kinetic trials was followed.

Kinetic Order in Carboxylate 1a (see SI): The kinetic order in carboxylate was determined by studying the initial rate of the reaction with different concentrations of **1a** (0.1 – 0.3 M). **NOTE:** None of these reactions were homogenous so these results are inconclusive. General procedure A for kinetic trials was followed.

Indole Additive Screens (Table 3). Example given for 4-chloro-*N*-methylindole (**2j**) as the additive. A stock solution was prepared in a glovebox. A 20 mL vial was charged with **2a** (34.5 mg, 0.250 mmol), **2j** (41.5 mg, 0.250 mmol), biphenyl (9.0 mg, 0.0625 mmol, internal standard) and dioxane (1.25 mL). Separate vials containing [Pd] catalysts (as described above in general procedure A for kinetic trials) were charged with **1a** (29.5-33.0 mg, ca.150 µmol) and an aliquot of the 4-chlorobenzonitrile solution (0.5 mL, 100 µmol). The vials were sealed with a Teflon-lined cap and removed from the glovebox. The vials were heated to

140 °C. After 24 hours, the reactions were cooled to room temperature. The reaction was diluted with DCM (ca. 2 mL). An aliquot of the reaction mixture was filtered through a short plug of silica gel and the silica gel was washed with DCM (2 mL). The filtrate was collected and analyzed by GC-FID. The reactions were run in duplicate and the average yield value, additive remaining, and starting material remaining are reported.

General Procedure for Indole Screens Characterized by ^{19}F NMR (Table 4). Example given for 7-chloroindole (**2i**). A stock solution was prepared in a glovebox. A 20 mL vial was charged with **2i** (106.4 mg, 0.700 mmol), 1-fluoronapthalene (25.9 mg, 0.175 mmol, internal standard) and dioxane (3.5 mL). Separate vials containing [Pd] catalysts (as described above in general procedure A for kinetic trials) were charged with **1a** (29.5-33.0 mg, ca.150 μmol) and an aliquot of the with **2i** solution (0.5 mL, 100 μmol). The vials were sealed with a Teflon-lined cap and removed from the glovebox. The vials were heated to 140 °C. After 24 hours, the reactions were cooled to room temperature. The reaction mixture was filtered through a short plug of silica. The silica gel was washed with EtOAc (ca. 2 mL). An aliquot of the filtered reaction mixture was collected and analyzed by ^{19}F NMR. The yield reported is the average of the yield values calculated from the two product peaks in the ^{19}F NMR spectrum. Yields by ^{19}F NMR can be misleading due to changes in the relaxation delay of the ^{19}F nuclei. For these compounds, yields appeared to be within 8% based on an analysis with purified materials where the ^{19}F and ^{1}H integrations could be compared.

Kinetic Order in COD (See SI): The kinetic order in 1,5-cyclooctadiene (COD) was determined by studying the initial rate of reaction with different concentrations of COD ranging from 0- 0.02 M. Example given for experiment between aryl chloride **2a** and **1a** at $[COD]_0$ = 0.002 M. A stock solution was prepared in a glovebox. A 20 mL vial was charged with aryl chloride **2a** (290.0 mg, 2.68 mmol), biphenyl (82.2 mg, 533 μmol, internal standard) and dioxane (8.4 mL). A second 20 mL vial was charged with COD (3.1 mg, 28.7 μmol) and dioxane (3.0 mL). **NOTE:** for each [COD] investigated, a new stock solution was prepared with a different mass of COD so that all other variables would remain constant. Separate vials containing [Pd] catalysts (as described above in general procedure A for kinetic trials) were charged with **1a** (29.0-33.0 mg, ca. 150 μmol). Each vial was subsequently charged with an aliquot of the COD solution (0.1 mL, 1 μmol) followed by an aliquot of the **2a** solution (0.4 mL, 100 μmol). The vials were sealed with a Teflon-lined cap and removed from the glovebox.

Pre-Catalyst and Additives Loading Screens (Scheme 7): General procedures A or B were followed depending on the pre-catalysts used. Minor modifications were followed as specified above when XPhos or COD were used as additives.

TON Experiments (Table 5): Example given for 0.3 mol % XPhosPdG2 and 1 mol % COD. A stock solution was prepared in a glovebox. A 20 mL vial was charged with aryl chloride **2b** (358 mg, 2.51 mmol), biphenyl (104 mg, 0.671 mmol, internal standard) and dioxane (10 mL). A second 20 mL vial was charged with COD (16.2 mg, 150 μmol) and dioxane (15 mL). Separate vials containing 0.3 mol % XPhosPdG2 catalyst (as described above) were charged with **1a** (29.0-33.0 mg, ca. 150 μmol). Each vial was subsequently charged with an aliquot of the COD solution (0.1 mL, 1 μmol) followed by an aliquot of the **2b** solution (0.4 mL, 100 μmol). The vials were sealed with a Teflon-lined cap and removed from the glovebox. The vials were heated to 140 °C. After 24 h, the reactions were quenched by submerging the vial into an ice bath. The reaction was diluted with DCM (ca. 2 mL). An aliquot of the reaction mixture was filtered through a short plug of silica gel and the silica gel was washed with DCM (2 mL). The filtrate was collected and analyzed by GC-FID.

4'-(tert-butyl)-2,4,6-trifluoro-1,1'-biphenyl: ***General Procedure A for Decarboxylative Cross-Coupling.*** Compound **S3a** was synthesized via reported conditions with minor modifications.[5] Under air, a 20 mL vial was charged with XPhosPdG2 (7.9 mg, 0.010 mmol). The vial was brought into a glovebox, and charged with **1a** (222 mg, 1.50 mmol). A separate 20 mL vial was charged with 4-*tert*-butyl-chlorobenzene (253 mg, 1.50 mmol) and 1,4-dioxane (7.5 mL) to prepare a stock solution. An aliquot of this stock solution (5 mL) was added to the previous 20 mL reaction vial. The 20 mL vial was sealed tightly with a Teflon lined cap, brought out of the glove box and stirred at 140 °C. After 24 hours, the reaction was cooled to rt. The reactions were filtered through a short plug of silica gel and the silica gel was washed with EtOAc (60 mL). The filtrate was concentrated under reduced pressure. Final purification by column chromatography (gradient EtOAc/hexanes from 0% - 20%) afforded compound **S3a** as a waxy white solid (199 mg, 75%). ^{1}H NMR (400MHz, $CDCl_3$): δ 7.50 (m, 2H), 7.39 (m, 2H), 6.78 (m, 2H), 1.39 (s, 9H). ^{13}C{1H} NMR (126 MHz, $CDCl_3$): δ 161.6 (dt, J_{C-F} = 248.8, 15.7 Hz), 160.4 (ddd, J_{C-F} = 249.3, 14.6, 10.0 Hz), 151.4, 130.0 (m, J_{C-F} = 2.1 Hz), 125.4, 115.0 (td, J = 19.2, 4.8 Hz), 100.8 – 100.1 (m, 2C), 34.7, 31.3.^{19}F NMR (376 MHz, $CDCl_3$): δ -109.64 (t, J = 5.8 Hz, 1F), -111.33 (d, J = 6.0 Hz, 2F). IR (NaCl, thin film, cm^{-1}): 3094, 2963, 1438, 1118, 834, 513. HRMS (EI-TOF) *m/z*: $[M]^+$ calculated for $C_{16}H_{15}F_3^+$: 264.1120; Observed: 264.1130.

1-tosyl-6-(2,4,6-trifluorophenyl)-1H-indole (S3h). ***General Procedure B for Decarboxylative Cross-Coupling:*** Compound **S3h** was synthesized via reported conditions with minor modifications.[5] Under air, a 20 mL vial was charged with XPhosPdG2 (4.0 mg, 5.1 μmol) and 6-chloro-1-tosyl-1H-indole (156 mg, 0.509 mmol). The vial was brought into a glovebox, and charged with sodium 2,4,6-triflourobenzoate (150 mg, 0.756 mmol) and dioxane (2.5 mL). The 20 mL vial was sealed tightly with a Teflon lined cap, brought out of the glove box and heated to 140 °C. After 24 h, the reaction was cooled to rt. The reactions were filtered through a short plug of silica gel and the silica gel was washed with EtOAc (60 mL). The filtrate was concentrated under reduced pressure. Final purification by column chromatography (10% EtOAc/hexanes) afforded compound **S3h** as a crystalline white solid (171 mg, 84%). The reaction was run in duplicate (179 mg, 87%). The average of 86% is reported. ^{1}H NMR (500 MHz, $CDCl_3$): δ 8.20 (s, 1H), 7.85 (d, J = 8.5 Hz, 2H), 7.67 (d, J = 3.7 Hz, 1H), 7.60 (d, J = 8.1 Hz, 1H), 7.32 (dd, J = 8.1, 1.5 Hz, 1H), 7.23 (d, J = 8.4 Hz, 2H), 6.85 (dd, J = 8.1, 8.1 Hz, 2H), 6.70 (d, J = 3.7 Hz, 1H), 2.32 (s, 3H). ^{13}C{1H} NMR (126 MHz, $CDCl_3$): δ 161.8 (dt, J_{C-F} = 249.4, 15.5 Hz), 160.4 (ddd, J_{C-F} = 249.3, 14.6, 9.5 Hz), 145.2, 135.0, 134.7, 130.8, 129.9, 127.3, 127.0, 125.5, 124.5, 121.3, 115.6, 115.2 (td, J_{C-F} = 18.9, 4.5 Hz), 109.0, 101.0 – 100.3 (m), 21.5. ^{19}F NMR (376 MHz, $CDCl_3$): δ -108.78 (t, J = 5.9 Hz, 1F), -111.23 (d, J = 6.1 Hz, 2F). IR (NaCl, thin film, cm^{-1}): 3110, 2925, 1638, 1508, 1443, 1121, 1000. HRMS (ESI-TOF) *m/z*: $[M+Na]^+$ Calculated for $C_{21}H_{14}F_3NNaO_2S^+$: 424.0590; Observed: 424.0597, m.p (°C): 146-148.

4-(2,4,6-trifluorophenyl)-1H-indole (3j): General procedure A for decarboxylative cross-coupling was followed with minor modifications. The reaction was run with 10 mol % XPhosPdG2 (39.1 mg, 49.7 μmol) Final purification by column chromatography (30% MTBE/1% TEA/hexanes) afforded compound **3j** as an off-white waxy solid (67.2 mg, 54%). The reaction was run in duplicate (68.0 mg, 54%). The average of 54% is reported. ^{1}H NMR (500 MHz, $CDCl_3$): δ 8.19 (s, 1H), 7.47 (d, J = 8.2 Hz, 1H), 7.34 (dd, J = 8.0, 7.5 Hz, 1H), 7.24 (dd, J = 3.3, 2.4 Hz, 1H), 7.21 (d, J = 7.3 Hz, 1H), 6.87 (dd, J = 8.9, 7.4 Hz, 2H), 6.39 (s, 1H).^{13}C{1H} NMR (126 MHz, $CDCl_3$): δ 162.0 (dt, J_{C-F} = 248.5, 15.4 Hz), 160.7 (ddd, J_{C-F} = 249.6, 14.8, 10.2 Hz), 135.9, 127.5, 124.8, 122.2, 121.8, 120.5, 114.0 (td, J_{C-F} = 20.9, 4.7 Hz), 111.7, 102.1, 100.8 – 99.9 (m). ^{19}F NMR (376 MHz, $CDCl_3$): δ -108.71 (d, J = 6.1 Hz, 2F), -109.46 (t, J = 5.9 Hz, 1F).IR (NaCl, thin film, cm^{-1}): 3416, 3093, 1714, 1637, 1598, 1027. HRMS (ESI-TOF) *m/z*: $[M+H]^+$ Calculated for $C_{14}H_9F_3NO^+$: 248.0682; Observed: 248.0683.

7-(2,4,6-trifluorophenyl)-1H-indole (3i): General procedure B for decarboxylative cross-coupling was followed with minor modifications. The reaction was run with 10 mol % XPhosPdG2 (40.1 m, 50.9 μmol). Final purification by column chromatography (15% MTBE/1% TEA/pentane) afforded compound **3i** as a thick oil (42.6 mg, 35%). The reaction was run in duplicate (45.7 mg, 36%). The average of 36% is reported.^{1}H NMR (500 MHz, $CDCl_3$): δ 8.01 (s, 1H), 7.77 (dd, J = 5.7, 3.2 Hz, 1H), 7.28 – 7.22 (m, 3H), 6.89 (dd, J = 8.7, 7.4 Hz, 2H), 6.67 (dd, J = 3.3, 2.1 Hz, 1H). ^{13}C{1H} NMR (126 MHz, $CDCl_3$): δ 162.3 (dt, J_{C-F} = 249.7, 15.1 Hz), 160.7 (ddd, J_{C-F} = 250.4, 15.0, 9.9 Hz), 134.3, 128.4, 124.5, 124.4, 121.6, 119.7, 111.8 (td, J_{C-F} = 20.9, 4.8 Hz), 111.4, 103.1, 101.1 – 100.6 (m). ^{19}F NMR (376 MHz, $CDCl_3$): δ -107.93 (d, J = 6.2 Hz, 2F), -108.25 (t, J = 6.2 Hz, 1F). IR (NaCl, thin film, cm^{-1}): 3430, 3101, 2973, 1716, 1638, 1595, 1122. HRMS (ESI-TOF) *m/z*: $[M+H]^+$ Calculated for $C_{14}H_9F_3NO^+$: 248.0682; Observed: 248.0686.

5-(2,4,6-trifluorophenyl)-1H-indole (3e) ***General Procedure for Tosyl Deprotection:*** A 20 mL vial was charged with indole **3c** (357 mg, 0.890 mmol), methanol (10 mL, 0.089 M), NaOH (5 mL, 2 M aq, 10 mmol), sealed, and heated to 80 °C. After 2 h, the vial was cooled to rt and partially concentrated under reduced pressure (ca. 1/3 original volume). The mixture was the diluted with water (10 mL) and extracted with EtOAc (3 X 20 mL). The combined organic layers were washed with brine (30 mL), dried ($MgSO_4$), filtered, and concentrated under reduced pressure. Final purification by column chromatography (15% EtOAc/1% TEA/hexanes) afforded compound **3e** as a colorless solid (192 mg, 87%). ^{1}H NMR (400 MHz, $CDCl_3$): δ 8.08 (s, 1H), 7.82 (s, 1H), 7.44 (d, J = 8.4 Hz, 1H), 7.33 (dd, J = 8.4, 1.6 Hz, 1H), 7.22 (t, J = 2.8 Hz, 1H), 6.87 (dd, J = 8.0, 8.0 Hz, 2H), 6.68 (t, J = 2.7 Hz, 1H). ^{13}C{1H} NMR (126 MHz, $CDCl_3$): δ 161.4 (dt, J_{C-F} = 248.0, 15.6 Hz), 160.6 (ddd, J_{C-F} = 248.1, 14.7, 9.9 Hz), 135.6, 128.0, 125.1, 124.2, 122.8, 119.6, 116.2 (td, J_{C-F} = 19.6, 4.7 Hz), 111.1, 103.0, 101.0 – 99.9 (m). ^{19}F NMR (376 MHz, $CDCl_3$): δ -110.22 (t, J = 5.7 Hz, 1F), -111.19 (d, J = 5.5 Hz, 2F). IR (NaCl, thin film, cm^{-1}): 3421, 1596, 1460, 1424, 1016. HRMS (ESI-TOF) *m/z*: $[M+H]^+$ Calculated for $C_{14}H_9F_3NO^+$: 248.0682 Observed: 248.0683, m.p. (°C): 112-114.

6-(2,4,6-trifluorophenyl)-1H-indole (3h): The general procedure for tosyl deprotection was followed with minor modifications. The reaction was heated for 3 h and was conducted on a smaller scale (0.260 mmol). Final purification by column chromatography (15% EtOAc/1% TEA/hexanes) afforded compound **3h** as a crystalline white solid (64.2 mg, 70%). ^{1}H NMR (400 MHz, $CDCl_3$): δ 8.16 (s, 1H), 7.77 (d, *J* = 8.2 Hz, 1H), 7.47 (s, 1H), 7.30 – 7.19 (m, 2H), 6.82 (dd, *J* = 8.1, 8.1 Hz, 2H), 6.64 (t, *J* = 2.8 Hz, 1H). ^{13}C{1H} NMR (126 MHz, $CDCl_3$): δ 161.4 (dt, $J_{C\text{-}F}$ = 248.5, 15.6 Hz), 160.4 (ddd, $J_{C\text{-}F}$ = 248.6, 14.8, 9.8 Hz), 135.6, 127.9, 125.3, 122.1, 121.7, 120.6, 116.0 (td, $J_{C\text{-}F}$ = 19.4, 4.7 Hz), 113.0, 102.7, 100.8 – 100.0 (m). ^{19}F NMR (376 MHz, $CDCl_3$): δ -110.02 (t, *J* = 5.7 Hz, 1F), -111.11 (d, *J* = 5.6 Hz, 2F). IR (NaCl, thin film, cm^{-1}): 3419, 2092, 1595, 1434, 1018. HRMS (ESI-TOF) *m/z*: $[M+H]^+$ Calculated for $C_{14}H_9F_3NO^+$: 248.0682; Observed: 248.0673. m.p (°C): 149-153.

1-methyl-5-(2,4,6-trifluorophenyl)-1H-indole (3d): A 20 mL vial was charged with indole **3e** (86.3 mg, 0.249 mmol) and THF (1.2 mL, 0.2 M) and cooled in an ice bath. The vial was charged with NaH (22.7 mg, 60 wt % in mineral oil, 0.568 mmol). After 10 min, methyl iodide (0.05 mL, 0.80 mmol) was added dropwise. The reaction was allowed to gradually warm to rt. After 18 h, the reaction was quenched by pouring the mixture onto ammonium chloride (10 mL, sat. aq.). The resulting solution was extracted with EtOAc (3 X 20 mL). The combined organic layers were sequentially washed with NaOH (30 mL, 2M aq.), brine (30 mL), dried ($MgSO_4$), filtered, and concentrated under reduced pressure. Product **3d** was isolated as a pink crystalline solid (91.2 mg, >99%) without further purification. ^{1}H NMR (400 MHz, $CDCl_3$): δ 7.78 (s, 1H), 7.46 (d, *J* = 8.5 Hz, 1H), 7.35 (dd, *J* = 8.5, 1.5 Hz, 1H), 7.14 (d, *J* = 3.2 Hz, 1H), 6.85 (dd, *J* = 8.8, 7.7 Hz, 2H), 6.62 (dd, *J* = 3.1, 0.9 Hz, 1H), 3.85 (s, 3H). ^{13}C{1H} NMR (126 MHz, $CDCl_3$): δ 161.3 (dt, $J_{C\text{-}F}$ = 247.8, 15.5 Hz), 160.6 (ddd, $J_{C\text{-}F}$ = 248.1, 14.6, 9.8 Hz), 136.5, 129.6, 128.5, 123.7, 123.0, 119.1, 116.3 (td, $J_{C\text{-}F}$ = 19.6, 4.8 Hz), 109.2, 101.4, 100.6 – 100.0 (m), 32.9. ^{19}F NMR (376 MHz, $CDCl_3$): δ -110.46 (t, *J* = 5.5 Hz, 1F), -111.18 (d, *J* = 5.8 Hz, 2F). IR (NaCl, thin film, cm^{-1}): 2924, 2854, 1636, 1594, 1424, 1026. HRMS (ESI-TOF) *m/z*: $[M+H]^+$ Calculated for $C_{15}H_{11}F_3N^+$: 262.0838; Observed: 262.0840. m.p. . (°C): 133-134.

1-(5-(2,4,6-trifluorophenyl)-1H-indol-1-yl)ethan-1-one (3f): A 20 mL vial was charged with indole **3e** (52.8 mg, 0.214 mmol), DCE (1 mL, 0.2 M), TEA (0.05 mL, 0.4 mmol), acetic anhydride (0.05 mL, 0.6 mmol), and DMAP (6.0 mg, 49 μmol). The vial was sealed and heated to 80 °C. After 3 h, the vial was cooled to rt. The reaction was quenched by pouring the mixture onto water. The resulting mixture was extracted with EtOAc (3 X 20 mL). The combined organic layers were washed with brine (30 mL), dried ($MgSO_4$), filtered, and concentrated under reduced pressure. Final purification by column chromatography (15% EtOAc/hexanes) afforded compound **3f** as a waxy white solid (56.6 mg, 92%). ^{1}H NMR (400 MHz, $CDCl_3$): δ 8.55 (d, *J* = 8.6 Hz, 1H), 7.65 (s, 1H), 7.50 – 7.39 (m, 2H), 6.80 (dd, *J* = 8.8, 7.8 Hz, 2H), 6.69 (d, *J* = 3.5 Hz, 1H), 2.66 (s, 3H). ^{13}C{1H} NMR (126 MHz, $CDCl_3$): δ 168.7, 161.7 (dt, $J_{C\text{-}F}$ = 248.9, 15.6 Hz), 160.4 (ddd, $J_{C\text{-}F}$ = 249.0, 14.7, 9.7 Hz), 135.3, 130.5, 127.2, 125.9, 123.6, 122.8, 116.5, 115.2 (td, $J_{C\text{-}F}$ = 19.4, 4.7 Hz), 109.2, 100.76 – 100.14 (m), 23.9.^{19}F NMR (376 MHz, $CDCl_3$): δ -109.3 (t, *J* = 6.0 Hz, 1F), -111.3 (d, *J* = 5.8 Hz, 2F). IR (NaCl, thin film, cm^{-1}): 3108, 1709, 1636, 1504, 1171, 1025. HRMS (ESI-TOF) *m/z*: $[M+Na]^+$ Calculated for $C_{16}H_{10}F_3NNaO^+$: 312.0607; Observed: 312.0615.

2,2-dimethyl-1-(5-(2,4,6-trifluorophenyl)-1H-indol-1-yl)propan-1-one (3g): A 20 mL vial was charged with indole **3e** (74.7 mg, 0.301 mmol), DCM (3 mL, 0.1 M), TEA (0.16 mL, 1.1 mmol), and cooled in an ice bath. The vial was charged with DMAP (4.1 mg, 33 μmol) and PivCl (0.10 mL, 0.81 mmol) was added dropwise. The reaction was allowed to gradually warm to rt. After 18 h, the reaction was poured onto water and extracted with EtOAc (3 X 20 mL). The combined organic layers were washed with brine (30 mL), dried ($MgSO_4$), filtered, and concentrated under reduced pressure. Final purification by column chromatography (10% EtOAc/hexanes) afforded compound **3g** as a white solid (67.4 mg, 67%). ^{1}H NMR (400 MHz, $CDCl_3$): δ 8.63 (d, *J* = 8.7 Hz, 1H), 7.81 (d, *J* = 3.8 Hz, 1H), 7.65 (s, 1H), 7.43 (dq, *J* = 8.7, 1.5 Hz, 1H), 6.80 (dd, *J* = 7.9, 7.9 Hz, 2H), 6.69 (d, *J* = 3.5 Hz, 1H), 1.56 (s, 9H). ^{13}C{1H} NMR (126 MHz, $CDCl_3$): δ 177.1, 161.6 (dt, $J_{C\text{-}F}$ = 248.8, 15.4 Hz), 160.4 (ddd, $J_{C\text{-}F}$ = 249.0, 14.7, 9.7 Hz), 136.5, 129.5, 127.2, 126.3, 123.5, 122.4, 117.3, 115.3 (td, $J_{C\text{-}F}$ = 19.3, 4.2 Hz), 108.3, 100.7 – 100.1 (m), 41.3, 28.7. ^{19}F NMR (376 MHz, $CDCl_3$): δ -109.5 (t, *J* = 5.8 Hz, 1F), -111.2 (d, *J* = 5.8 Hz, 2F). IR (NaCl, thin film, cm^{-1}): 3105, 2977, 1696, 1637, 1614, 1218. HRMS (ESI-TOF) *m/z*: $[M+Na]^+$ Calculated for $C_{19}H_{16}F_3NNaO^+$: 354.1076; Observed: 354.1077. m.p. (°C): 135-136.

Note: All other cross-coupled products were synthesized as described in our previous report. The procedures and characterization data can be found there. [68]

■ **Computational Methods**

Calculations were performed with Gaussian 16.[69] An ultrafine integration grid and the keyword 5d were used for all calculations. Geometry optimizations of stationary points were carried out in the gas phase with the M06L[70] functional with BS1 (BS1 = the LANL2DZ[93] pseudopotential for Pd, the 6-31+G(d) basis set for O and Cl, and the 6-31G(d) basis set for all other atoms). Frequency analyses were carried out at the same level to evaluate the zero-point vibrational energy and thermal corrections at 413.15 K. Gibbs free energy values are reported after applying Cramer and Truhlar's anharmonic correction to frequencies that are less than 100 cm^{-1}.[94] The nature of the stationary points was determined in each case according to the appropriate number of negative eigenvalues of the Hessian matrix. Forward and reverse intrinsic reaction coordinate calculations were carried out on the optimized transition structures to ensure that the TSs indeed connect the appropriate reactants and products.[95–97] Multiple conformations were considered for all structures, and the lowest energy conformations are reported. Single point energy calculations were performed on the gas-phase optimized geometries using the M06 functional with BS2 (BS2 = the SDD pseudopotential for Pd and the 6-311++G(2d,p) basis set for all other atoms). Bulk solvent effects in 1,4-dioxane were considered implicitly in the single point energy calculations through the CPCM continuum solvation model.[98]

Supporting Information.

The Supporting Information is available free of charge on the ACS Publications website at DOI: XX.

Experimental procedures, primary kinetic data, computational data, and spectral data (PDF)

AUTHOR INFORMATION

Corresponding Author

*jtopczew@umn.edu
*sharon.neufeldt@montana.edu

Notes

The authors declare no competing financial interests.

Author Contributions

The manuscript was written through contributions of all authors. All authors have given approval to the final version of the manuscript.

ACKNOWLEDGMENT

Financial support was provided by the National Science Foundation award number CHE1942223 (J.J.T. and R.A.D.). This material is based upon work supported by the National Science Foundation Graduate Research Fellowship (J.N.H.) under Grant No. CON-75851-00074041. A.S.M and S.R.N. are grateful to Montana State University for support. Calculations were performed on Comet at SDSC and Bridges/Bridges-2 at the Pittsburgh Supercomputing Center through XSEDE (CHE190050 and CHE170089), which is supported by NSF (ACI-1548562), as well as on the Hyalite High Performance Computing System at MSU.

REFERENCES

(1) Miyaura, N.; Suzuki, A. Palladium-Catalyzed Cross-Coupling Reactions of Organoboron Compounds. *Chem. Rev.* **1995**, *95*, 2457–2483. https://doi.org/10.1021/cr00039a007.

(2) Johansson Seechurn, C. C.; Kitching, M. O.; Colacot, T. J.; Snieckus, V. Palladium-Catalyzed Cross-Coupling: A Historical Contextual Perspective to the 2010 Nobel Prize. *Angew. Chemie. Int. Ed.* **2012**, *51*, 5062–5085. https://doi.org/10.1002/anie.201107017.

(3) Knapp, D. M.; Gillis, E. P.; Burke, M. D. A General Solution for Unstable Boronic Acids: Slow-Release Cross-Coupling from Air-Stable MIDA Boronates. *J. Am. Chem. Soc.* **2009**, *131*, 6961–6963. https://doi.org/10.1021/ja901416p.

(4) Lozada, J.; Liu, Z.; Perrin, D. M. Base-Promoted Protodeboronation of 2,6-Disubstituted Arylboronic Acids. *J. Org. Chem.* **2014**, *79*, 5365–5368. https://doi.org/10.1021/jo500734z.

(5) Cox, P. A.; Reid, M.; Leach, A. G.; Campbell, A. D.; King, E. J.; Lloyd-Jones, G. C. Base-Catalyzed Aryl-B(OH)2 Protodeboronation Revisited: From Concerted Proton Transfer to Liberation of a Transient Aryl Anion. *J. Am. Chem. Soc.* **2017**, *139*, 13156–13165. https://doi.org/10.1021/jacs.7b07444.

(6) Cox, P. A.; Leach, A. G.; Campbell, A. D.; Lloyd-Jones, G. C. Protodeboronation of Heteroaromatic, Vinyl, and Cyclopropyl Boronic Acids: PH-Rate Profiles, Autocatalysis, and Disproportionation. *J. Am. Chem. Soc.* **2016**, *138*, 9145–9157. https://doi.org/10.1021/jacs.6b03283.

(7) Rodríguez, N.; Gooßen, L. J. Decarboxylative Coupling Reactions: A Modern Strategy for C–C-Bond Formation. *Chem. Soc. Rev.* **2011**, *40*, 5030–5048. https://doi.org/10.1039/c1cs15093f.

(8) Patra, T.; Maiti, D.; Wei, Y.; Hu, P.; Zhang, M.; Su, W. Decarboxylation as the Key Step in C−C Bond-Forming Reactions. *Chem. Eur. J.* **2017**, *23*, 7382–7401. https://doi.org/10.1002/chem.201604496.

(9) Daley, R. A. R. A.; Topczewski, J. J. J. J. Aryl-Decarboxylation Reactions Catalyzed by Palladium: Scope and Mechanism. *Synthesis* **2020**, *51*, 365–377. https://doi.org/10.1055/s-0039-1690769.

(10) Gooßen, L. J.; Deng, G.; Levy, L. M. Synthesis of Biaryls via Catalytic Decarboxylative Coupling. *Science* **2006**, *313*, 662–664. https://doi.org/10.1126/science.1128684.

(11) Myers, A. G.; Tanaka, D.; Mannion, M. R. Development of a Decarboxylative Palladation Reaction and Its Use in a Heck-Type Olefination of Arene Carboxylates. *J. Am. Chem. Soc.* **2002**, *124*, 11250–11251. https://doi.org/10.1021/ja027523m.

(12) Cornella, J.; Larrosa, I. Decarboxylative Carbon-Carbon Bond-Forming Transformations of (Hetero)Aromatic Carboxylic Acids. *Synthesis* **2012**, *44*, 653–676. https://doi.org/10.1055/s-0031-1289686.

(13) Zhang, T.; Wang, N.-X. X.; Xing, Y. Advances in Decarboxylative Oxidative Coupling Reaction. *J. Org. Chem.* **2018**, *83*, 7559–7565. https://doi.org/10.1021/acs.joc.8b01080.

(14) Chen, L.; Ju, L.; Bustin, K. A.; Hoover, J. M. Copper-Catalyzed Oxidative Decarboxylative C-H Arylation of Benzoxazoles with 2-Nitrobenzoic Acids. *Chem. Commun.* **2015**, *51*, 15059–15062. https://doi.org/10.1039/c5cc06645j.

(15) Crovak, R. A.; Hoover, J. M. A Predictive Model for the Decarboxylation of Silver Benzoate Complexes Relevant to Decarboxylative Coupling Reactions. *J. Am. Chem. Soc.* **2018**, *140*, 2434–2437. https://doi.org/10.1021/jacs.7b13305.

(16) Honeycutt, A. P.; Hoover, J. M. Nickel-Catalyzed Oxidative Decarboxylative Annulation for the Synthesis of Heterocycle-Containing Phenanthridinones. *Org. Lett.* **2018**, *20*, 7216–7219. https://doi.org/10.1021/acs.orglett.8b03144.

(17) Honeycutt, A. P.; Hoover, J. M. Nickel-Catalyzed Oxidative Decarboxylative (Hetero)Arylation of Unactivated C-H Bonds: Ni and Ag Synergy. *ACS Catal.* **2017**, *7*, 4597–4601. https://doi.org/10.1021/acscatal.7b01683.

(18) Wei, Y.; Hu, P.; Zhang, M.; Su, W. Metal-Catalyzed Decarboxylative C-H Functionalization. *Chem. Rev.* **2017**, *117*, 8864–8907. https://doi.org/10.1021/acs.chemrev.6b00516.

(19) Gooßen, L. J.; Rodríguez, N.; Gooßen, K. Carboxylic Acids as Substrates in Homogeneous Catalysis Angewandte. *Angew. Chemie. Int. Ed.* **2008**, *47*, 3100–3120. https://doi.org/10.1002/anie.200704782.

(20) Gooßen, L. J.; Gooßen, K.; Rodríguez, N.; Blanchot, M.; Linder, C.; Zimmermann, B. New Catalytic Transformations of Carboxylic Acids. *Pure Appl. Chem.* **2008**, *80*, 1725–1733. https://doi.org/10.1351/pac200880081725.

(21) Hoover, J. M. Mechanistic Aspects of Copper-Catalyzed Decarboxylative Coupling Reactions of (Hetero)Aryl Carboxylic Acids. *Comments Inorg. Chem.* **2017**, *37*, 169–200. https://doi.org/10.1080/02603594.2016.1261023.

(22) Shi, W.; Liu, C.; Lei, A. Transition-Metal Catalyzed Oxidative Cross-Coupling Reactions to Form C-C Bonds Involving Organometallic Reagents as Nucleophiles. *Chem. Soc. Rev.* **2011**, *40*, 2761–2776. https://doi.org/10.1039/c0cs00125b.

(23) Dzik, W. I.; Lange, P. P.; Gooßen, L. J. Carboxylates as Sources of Carbon Nucleophiles and Electrophiles: Comparison of Decarboxylative and Decarbonylative Pathways. *Chem. Sci.* **2012**, *3*, 2671–2678. https://doi.org/10.1039/c2sc20312j.

(24) Prinsell, M. R.; Everson, D. A.; Weix, D. J. Nickel-Catalyzed, Sodium Iodide-Promoted Reductive Dimerization of Alkyl Halides, Alkyl Pseudohalides, and Allylic Acetates. *Chem. Commun.* **2010**, *46*, 5743–5745. https://doi.org/10.1039/c0cc01716g.

(25) Gooßen, L. J.; Rodríguez, N.; Linder, C.; Lange, P. P.; Fromm, A. Comparative Study of Copper- and Silver-Catalyzed Protodecarboxylations of Carboxylic Acids. *ChemCatChem* **2010**, *2*, 430–442. https://doi.org/10.1002/cctc.200900277.

(26) Xue, L.; Su, W.; Lin, Z. Mechanism of Silver- and Copper-Catalyzed Decarboxylation Reactions of Aryl Carboxylic Acids. *Dalt. Trans.* **2011**, *40*, 11926–11936. https://doi.org/10.1039/c1dt10771b.

(27) Baur, A.; Bustin, K. A.; Aguilera, E.; Petersen, J. L.; Hoover, J. M. Copper and Silver Benzoate and Aryl Complexes and Their Implications for Oxidative Decarboxylative Coupling Reactions. *Org. Chem. Front.* **2017**, *4*, 519–524. https://doi.org/10.1039/c6qo00678g.

(28) Fromm, A.; Van Wüllen, C.; Hackenberger, D.; Gooßen, L. J. Mechanism of Cu/Pd-Catalyzed Decarboxylative Cross-Couplings: A DFT Investigation. *J. Am. Chem. Soc.* **2014**, *136*, 10007–10023. https://doi.org/10.1021/ja503295x.

(29) Hackenberger, D.; Song, B.; Grünberg, M. F.; Farsadpour, S.; Menges, F.; Kelm, H.; Groß, C.; Wolff, T.; Niedner-Schatteburg, G.; Thiel, W. R.; Gooßen, L. J. Bimetallic Cu/Pd Catalysts with Bridging Aminopyrimidinyl Phosphines for Decarboxylative Cross-Coupling Reactions at Moderate Temperature. *Chem. Cat. Chem* **2015**, *7*, 3579–3588. https://doi.org/10.1002/cctc.201500769.

(30) Cahiez, G.; Moyeux, A.; Gager, O.; Poizat, M. Copper-Catalyzed Decarboxylation of Aromatic Carboxylic Acids: En Route to Milder Reaction Conditions. *Adv. Synth. Catal.* **2013**, *355*, 790–796. https://doi.org/10.1002/adsc.201201018.

(31) Green, K. A.; Hoover, J. M. Intermediacy of Copper(i) under Oxidative Conditions in the Aerobic Copper-Catalyzed Decarboxylative Thiolation of Benzoic Acids. *ACS Catal.* **2020**, *10*, 1769–1782. https://doi.org/10.1021/acscatal.9b04110.

(32) Cohen, T.; Berninger, R. W.; Wood, J. T. Products and Kinetics of Decarboxylation of Activated and Unactivated Aromatic Cuprous Carboxylates in Pyridine and in Quinoline. *J. Org. Chem.* **1978**, *43*, 837–848. https://doi.org/10.1021/jo00399a010.

(33) Tanaka, D.; Romeril, S. P.; Myers, A. G. On the Mechanism of the Palladium(II)-Catalyzed Decarboxylative Olefination of Arene Carboxylic Acids. Crystallographic Characterization of Non-Phosphine Palladium(II) Intermediates and Observation of Their Stepwise Transformation in Heck-like Processes. *J. Am. Chem. Soc.* **2005**, *127*, 10323–10333. https://doi.org/10.1021/ja052099l.

(34) Dickstein, J. S.; Curto, J. M.; Gutierrez, O.; Mulrooney, C. A.; Kozlowski, M. C. Mild Aromatic Palladium-Catalyzed Protodecarboxylation: Kinetic Assessment of the Decarboxylative Palladation and the Protodepalladation Steps. *J. Org. Chem.* **2013**, *78*, 4744–4761. https://doi.org/10.1021/jo400222c.

(35) Bilodeau, F.; Brochu, M. C.; Guimond, N.; Thesen, K. H.; Forgione, P. Palladium-Catalyzed Decarboxylative Cross-Coupling Reaction between Heteroaromatic Carboxylic Acids and Aryl Halides. *J. Org. Chem.* **2010**, *75*, 1550–1560. https://doi.org/10.1021/jo9022793.

(36) Shang, R.; Xu, Q.; Jiang, Y. Y.; Wang, Y.; Liu, L. Pd-Catalyzed Decarboxylative Cross Coupling of Potassium Polyfluorobenzoates Aryl Bromides, Chlorides, and Triflates. *Org. Lett.* **2010**, *12*, 1000–1003.

(37) Xie, H.; Lin, F.; Lei, Q.; Fang, W. Mechanism and Substrate-Dependent Rate-Determining Step in Palladium-Catalyzed Intramolecular Decarboxylative Coupling of Arenecarboxylic Acids with Aryl Bromides: A DFT Study. *Organometallics* **2013**, *32*, 6957–6968. https://doi.org/10.1021/om400503x.

(38) Forgione, P.; Brochu, M.; St-Onge, M.; Thesen, K. H.; Bailey, M. D.; Bilodeau, F. Unexpected Intermolecular Pd-Catalyzed Cross-Coupling Reaction Employing Heteroaromatic Carboxylic Acids as Coupling Partners. *J. Am. Chem. Soc.* **2006**, *126*, 11350–11351. https://doi.org/10.1021/ja063511f.

(39) Mitchell, D.; Coppert, D. M.; Moynihan, H. A.; Lorenz, K. T.; Kissane, M.; Mcnamara, O. A.; Maguire, A. R. A Practical Synthesis of Biaryls via a Thermal Decarboxylative Pd-Catalyzed Cross-Coupling Reaction Operating at Moderate Temperature. *Org. Process Res. Dev.* **2011**, *15*, 981–985. https://doi.org/10.1021/op200030t.

(40) Kissane, M.; Mcnamara, O. A.; Mitchell, D.; Coppert, D. M.; Moynihan, H. A.; Lorenz, K. T.; Maguire, A. R. Expanded Scope of Heterocyclic Biaryl Synthesis via a Palladium-Catalysed Thermal Decarboxylative Cross-Coupling Reaction. *Tetrahedron Lett.* **2012**, *53*, 403–405. https://doi.org/10.1016/j.tetlet.2011.11.051.

(41) Shen, Z.; Ni, Z.; Mo, S.; Wang, J.; Zhu, Y. Palladium-Catalyzed Intramolecular Decarboxylative Coupling of Arene Carboxylic Acids / Esters with Aryl Bromides. *Chem. Eur. J.* **2012**, *18*, 4859–4865. https://doi.org/10.1002/chem.201103438.

(42) Patra, T.; Maiti, D. Decarboxylation as the Key Step in C–C Bond-Forming Reactions. *Chem. Eur. J.* **2017**, *23*, 7382–7401. https://doi.org/10.1002/chem.201604496.

(43) Nakano, M.; Tsurugi, H.; Satoh, T.; Miura, M. Palladium-Catalyzed Perarylation of 3-Thiophene- and 3-Furancarboxylic Acids Accompanied by C - H Bond Cleavage and Decarboxylation. *Org. Lett.* **2008**, *10*, 1851–1854.

(44) Arroyave, F. A.; Reynolds, J. R. Conjugated Oligomers via Pd-Mediated Decarboxylative Cross Coupling. *Org. Lett.* **2010**, *12*, 1328–1331.

(45) Daley, R. A. R. A.; Liu, E. C. E.-C.; Topczewski, J. J. J. J. Additive-Free Palladium-Catalyzed Decarboxylative Cross-Coupling of Aryl Chlorides. *Org. Lett.* **2019**, *21*, 4734–4738. https://doi.org/10.1021/acs.orglett.9b01620.

(46) Hooker, L. V.; Neufeldt, S. R. Ligation State of Nickel during C–O Bond Activation with Monodentate Phosphines. *Tetrahedron* **2018**, *74*, 6717–6725. https://doi.org/10.1016/j.tet.2018.10.025.

(47) Bruno, N. C.; Tudge, M. T.; Buchwald, S. L. Design and Preparation of New Palladium Precatalysts for C-C and C-N Cross-Coupling Reactions. *Chem. Sci.* **2013**, *4*, 916–920. https://doi.org/10.1039/c2sc20903a.

(48) Ingoglia, B. T.; Buchwald, S. L. Oxidative Addition Complexes as Precatalysts for Cross-Coupling Reactions Requiring Extremely Bulky Biarylphosphine Ligands. *Org. Lett.* **2017**, *19*, 2853–2856. https://doi.org/10.1021/acs.orglett.7b01082.

(49) Espenson, J. H. *Chemical Kinetics and Reaction Mechanisms*; McGraw-Hill, Inc.: New York, 1995.

(50) Amatore, C.; Pflüger, F. Mechanism of Oxidative Addition of Palladium(0) with Aromatic Iodides in Toluene, Monitored at Ultramicroelectrodes. *Organometallics* **1990**, *9*, 2276–2282. https://doi.org/10.1021/om00158a026.

(51) Hartwig, J. F.; Paul, F. Oxidative Addition of Aryl Bromide after Dissociation of Phosphine from a Two-Coordinate Palladium(0) Complex, Bis(Tri-o-Tolylphosphine)Palladium(0). *J. Am. Chem. Soc.* **1995**, *117*, 5373–5374. https://doi.org/10.1021/ja00124a026.

(52) Yin, J.; Rainka, M. P.; Zhang, X. X.; Buchwald, S. L. A Highly Active Suzuki Catalyst for the Synthesis of Sterically Hindered Biaryls: Novel Ligand Coordination. *J. Am. Chem. Soc.* **2002**, *124*, 1162–1163. https://doi.org/10.1021/ja017082r.

(53) Christmann, U.; Vilar, R. Monoligated Palladium Species as Catalysts in Cross-Coupling Reactions. *Angew. Chemie. Int. Ed.* **2005**, *44*, 366–374. https://doi.org/10.1002/anie.200461189.

(54) Walker, S. D.; Barder, T. E.; Martinelli, J. R.; Buchwald, S. L. A Rationally Designed Universal Catalyst for Suzuki-Miyaura Coupling Processes. *Angew. Chemie. Int. Ed.* **2004**, *43*, 1871–1876. https://doi.org/10.1002/anie.200353615.

(55) Uehling, M. R.; King, R. P.; Krska, S. W.; Cernak, T.; Buchwald, S. L. Pharmaceutical Diversification via Palladium Oxidative Addition Complexes. *Science* **2019**, *363*, 405–408.

(56) Ruiz-Castillo, P.; Blackmond, D. G.; Buchwald, S. L. Rational Ligand Design for the Arylation of Hindered Primary Amines Guided by Reaction Progress Kinetic Analysis. *J. Am. Chem. Soc.* **2015**, *137*, 3085–3092. https://doi.org/10.1021/ja512903g.

(57) Hayashi, Y.; Wada, S.; Yamashita, M.; Nozaki, K. Syntheses and Thermolysis of Arylpalladium Hydroxide Complexes: Implications for C(Sp 2)-OH Bond-Forming Reductive Elimination to Generate Phenol Derivatives. *Organometallics* **2012**, *31*, 1073–1081. https://doi.org/10.1021/om201142s.

(58) Barder, T. E.; Biscoe, M. R.; Buchwald, S. L. Structural Insights into Active Catalyst Structures and Oxidative Addition to (Biaryl)Phosphine - Palladium Complexes via Density Functional Theory and Experimental Studies. *Organometallics* **2007**, *26*, 2183–2192. https://doi.org/10.1021/om0701017.

(59) Ingoglia, B. T.; Wagen, C. C.; Buchwald, S. L. Biaryl Monophosphine Ligands in Palladium-Catalyzed C–N Coupling: An Updated User's Guide. *Tetrahedron* **2019**, *75*, 4199–4211. https://doi.org/10.1016/j.tet.2019.05.003.

(60) Tsang, W. C. P.; Munday, R. H.; Brasche, G.; Zheng, N.; Buchwald, S. L. Palladium-Catalyzed Method for the Synthesis of Carbazoles via Tandem C-H Functionalization and C-N Bond Formation. *J. Org. Chem.* **2008**, *73*, 7603–7610. https://doi.org/10.1021/jo801273q.

(61) Lee, H. G.; Milner, P. J.; Buchwald, S. L. An Improved Catalyst System for the Pd-Catalyzed Fluorination of (Hetero)Aryl Triflates. *Org. Lett.* **2013**, *15*, 5602–5605. https://doi.org/10.1021/ol402859k.

(62) Park, N. H.; Vinogradova, E. V.; Surry, D. S.; Buchwald, S. L. Design of New Ligands for the Palladium-Catalyzed Arylation of α-Branched Secondary Amines. *Angew. Chemie. Int. Ed.* **2015**, *54*, 8259–8262. https://doi.org/10.1002/anie.201502626.

(63) Bruno, N. C.; Niljianskul, N.; Buchwald, S. L. N-Substituted 2-Aminobiphenylpalladium Methanesulfonate Precatalysts and Their Use in C-C and C-N Cross-Couplings. *J. Org. Chem.* **2014**, *79*, 4161–4166. https://doi.org/10.1021/jo500355k.

(64) Amatore, C.; Carré, E.; Jutand, A.; M'Barki, M. A.; Meyer, G. Evidence for the Ligation of Palladium(0) Complexes by Acetate Ions: Consequences on the Mechanism of Their Oxidative Addition with Phenyl Iodide and PhPd(OAc)(PPh3)2 as Intermediate in the Heck Reaction. *Organometallics* **1995**, *14*, 5605–5614. https://doi.org/10.1021/om00012a029.

(65) Amatore, C.; Jutand, A.; Thuilliez, A. Formation of Palladium(0) Complexes from Pd(OAc)2 and a Bidentate Phosphine Ligand (Dppp) and Their Reactivity in Oxidative Addition. *Organometallics* **2001**, *20*, 3241–3249. https://doi.org/10.1021/om0101137.

(66) Amatore, C.; Jutand, A.; M'Barki, M. A. Evidence of the Formation of Zerovalent Palladium from Pd(OAc)2 and Triphenylphosphine. *Organometallics* **1992**, *11*, 3009–3013. https://doi.org/10.1021/om00045a012.

(67) Eyring, H. The Activated Complex in Chemical Reactions. *J. Chem. Phys.* **1935**, *107*, 107–115. https://doi.org/10.1063/1.1749604.

(68) Daley, R. A.; Liu, E.-C.; Topczewski, J. J. Additive-Free Palladium-Catalyzed Decarboxylative Cross-Coupling of Aryl Chlorides. *Org. Lett.* **2019**, *21* (12). https://doi.org/10.1021/acs.orglett.9b01620.

(69) M. J. Frisch, G. W. Trucks, H. B. Schlegel, G. E. Scuseria, M. A. Robb, J. R. Cheeseman, G. Scalmani, V. Barone, G. A. Petersson, H. Nakatsuji, X. Li, M. Caricato, A. Marenich, J. Bloino, B. G. Janesko, R. Gomperts, B. Mennucci, H. P. Hratchian, J. V. Ort, and D. J. F. Gaussian, Inc., Wallingford CT. 2016.

(70) Yu, H. S.; He, X.; Truhlar, D. G. MN15-L: A New Local Exchange-Correlation Functional for Kohn-Sham Density Functional Theory with Broad Accuracy for Atoms, Molecules, and Solids. *J. Chem. Theory Comput.* **2016**, *12*, 1280–1293. https://doi.org/10.1021/acs.jctc.5b01082.

(71) Hossian, A.; Bhunia, S. K.; Jana, R. Substrate-Dependent Mechanistic Divergence in Decarboxylative Heck Reaction at Room Temperature. *J. Org. Chem.* **2016**, *81*, 2521–2533. https://doi.org/10.1021/acs.joc.6b00100.

(72) Vitaku, E.; Smith, D. T.; Njardarson, J. T. Analysis of the Structural Diversity, Substitution Patterns, and Frequency of Nitrogen Heterocycles among U.S. FDA Approved Pharmaceuticals. *J. Med. Chem.* **2014**, *57*, 10257–10274. https://doi.org/10.1021/jm501100b.

(73) Kutchukian, P. S.; Dropinski, J. F.; Dykstra, K. D.; Li, B.; Dirocco, D. A.; Streckfuss, E. C.; Campeau, L. C.; Cernak, T.; Vachal, P.; Davies, I. W.; Krska, S. W.; Dreher, S. D. Chemistry Informer Libraries: A Chemoinformatics Enabled Approach to Evaluate and Advance Synthetic Methods. *Chem. Sci.* **2016**, *7*, 2604–2613. https://doi.org/10.1039/c5sc04751j.

(74) Düfert, M. A.; Billingsley, K. L.; Buchwald, S. L. Suzuki-Miyaura Cross-Coupling of Unprotected, Nitrogen-Rich Heterocycles: Substrate Scope and Mechanistic Investigation. *J. Am. Chem. Soc.* **2013**, *135*, 12877–12885. https://doi.org/10.1021/ja4064469.

(75) Ahneman, D. T.; Estrada, J. G.; Lin, S.; Dreher, S. D.; Doyle,

A. G. Predicting Reaction Performance in C–N Cross-Coupling Using Machine Learning. *Science* **2018**, *360*, 186–190.

(76) Smith, G. B.; Dezeny, G. C.; Hughes, D. L.; King, A. O.; Verhoeven, T. R. Mechanistic Studies of the Suzuki Cross-Coupling Reaction. *J. Org. Chem.* **1994**, *59*, 8151–8156. https://doi.org/10.1021/jo00105a036.

(77) Slagt, V. F.; De Vries, A. H. M.; De Vries, J. G.; Kellogg, R. M. Practical Aspects of Carbon-Carbon Cross-Coupling Reactions Using Heteroarenes. *Org. Process Res. Dev.* **2010**, *14*, 30–47. https://doi.org/10.1021/op900221v.

(78) Beletskaya, I. P.; Cheprakov, A. V. The Complementary Competitors: Palladium and Copper in C-N Cross-Coupling Reactions. *Organometallics* **2012**, *31*, 7753–7808. https://doi.org/10.1021/om300683c.

(79) Collins, K. D.; Glorius, F. A Robustness Screen for the Rapid Assessment of Chemical Reactions. *Nat. Chem.* **2013**, *5*, 597–601. https://doi.org/10.1038/nchem.1669.

(80) Gensch, T.; Teders, M.; Glorius, F. Approach to Comparing the Functional Group Tolerance of Reactions. *J. Org. Chem.* **2017**, *82*, 9154–9159. https://doi.org/10.1021/acs.joc.7b01139.

(81) Sandtorv, A. H. Transition Metal-Catalyzed C-H Activation of Indoles. *Adv. Synth. Catal.* **2015**, *357*, 2403–2435. https://doi.org/10.1002/adsc.201500374.

(82) Cornella, J.; Lu, P.; Larrosa, I. Intermolecular Decarboxylative Direct C-3 Arylation of Indoles with Benzoic Acids. *Org. Lett.* **2009**, *11*, 5506–5509. https://doi.org/10.1021/ol902304n.

(83) Miyasaka, M.; Fukushima, A.; Satoh, T.; Hirano, K. Fluorescent Diarylindoles by Palladium-Catalyzed Direct and Decarboxylative Arylations of Carboxyindoles. *Chem. Eur. J.* **2009**, *15*, 3674–3677. https://doi.org/10.1002/chem.200900098.

(84) Nandi, D.; Jhou, Y. M.; Lee, J. Y.; Kuo, B. C.; Liu, C. Y.; Huang, P. W.; Lee, H. M. Pd(0)-Catalyzed Decarboxylative Coupling and Tandem C-H Arylation/Decarboxylation for the Synthesis of Heteroaromatic Biaryls. *J. Org. Chem.* **2012**, *77*, 9384–9390. https://doi.org/10.1021/jo3015837.

(85) Yang, Y.; Oldenhuis, N. J.; Buchwald, S. L. Mild and General Conditions for Negishi Cross-Coupling Enabled by the Use of Palladacycle Precatalysts. *Angew. Chemie* **2013**, *125*, 643–647. https://doi.org/10.1002/ange.201207750.

(86) Tromp, M.; Sietsma, J. R. A.; Van Bokhoven, J. A.; Van Strijdonck, G. P. F.; Van Haaren, R. J.; Van der Eerden, A. M. J.; Van Leeuwen, P. W. N. M.; Koningsberger, D. C. Deactivation Processes of Homogeneous Pd Catalysts Using in Situ Time Resolved Spectroscopic Techniques. *Chem. Commun.* **2003**, 128–129. https://doi.org/10.1039/b206758g.

(87) Crabtree, R. H. Deactivation in Homogeneous Transition Metal Catalysis: Causes, Avoidance, and Cure. *Chem. Rev.* **2015**, *115*, 127–150. https://doi.org/10.1021/cr5004375.

(88) Gaikwad, A. V.; Rothenberg, G. In-Situ UV-Visible Study of Pd Nanocluster Formation in Solution. *Phys. Chem. Chem. Phys.* **2006**, *8*, 3669–3675. https://doi.org/10.1039/b604665g.

(89) Fiddy, S. G.; Evans, J.; Neisius, T.; Newton, M. A.; Tsoureas, N.; Tulloch, A. A. D.; Danopoulos, A. A. Comparative Experimental and EXAFS Studies in the Mizoroki-Heck Reaction with Heteroatom-Functionalised N-Heterocyclic Carbene Palladium Catalysts. *Chem. Eur. J.* **2007**, *13*, 3652–3659. https://doi.org/10.1002/chem.200601278.

(90) Fairlamb, I. J. S.; Kapdi, A. R.; Lee, A. F.; McGlacken, G. P.; Weissburger, F.; De Vries, A. H. M.; Schmieder-Van De Vondervoort, L. Exploiting Noninnocent (E,E)-Dibenzylideneacetone (Dba) Effects in Palladium(0)-Mediated Cross-Coupling Reactions: Modulation of the Electronic Properties of Dba Affects Catalyst Activity and Stability in Ligand and Ligand-Free Reaction Systems. *Chem. Eur. J.* **2006**, *12*, 8750–8761. https://doi.org/10.1002/chem.200600473.

(91) Fairlamb, I. J. S.; Kapdi, A. R.; Lee, A. F. H2-Dba Complexes of Pd(0): The Substituent Effect in Suzuki-Miyaura Coupling. *Org. Lett.* **2004**, *6*, 4435–4438. https://doi.org/10.1021/ol048413i.

(92) Amatore, C.; Jutand, A. Role of Dba in the Reactivity of Palladium(0) Complexes Generated in Situ from Mixtures of Pd(Dba)2 and Phosphines. *Coord. Chem. Rev.* **1998**, *178–180*, 511–528. https://doi.org/10.1016/s0010-8545(98)00073-3.

(93) Hay, P. J.; Wadt, W. R. Ab Initio Effective Core Potentials for Molecular Calculations. Potentials for K to Au Including the Outermost Core Orbitale. *J. Chem. Phys.* **1985**, *82*, 299–310. https://doi.org/10.1063/1.448975.

(94) Ribeiro, R. F.; Marenich, A. V.; Cramer, C. J.; Truhlar, D. G. Use of Solution-Phase Vibrational Frequencies in Continuum Models for the Free Energy of Solvation. *J. Phys. Chem. B* **2011**, *115*, 14556–14562. https://doi.org/10.1021/jp205508z.

(95) Gonzalez, C.; Bernhard Schlegel, H. An Improved Algorithm for Reaction Path Following. *J. Chem. Phys.* **1989**, *90*, 2154–2161. https://doi.org/10.1063/1.456010.

(96) Fukui, K. The Path of Chemical Reactions - The IRC Approach. *Acc. Chem. Res.* **1981**, *14*, 363–368. https://doi.org/10.1021/ar00072a001.

(97) Gonzalez, C.; Schlegel, H. B. Reaction Path Following in Mass-Weighted Internal Coordinates. *J. Phys. Chem.* **1990**, *94*, 5523–5527. https://doi.org/10.1021/j100377a021.

(98) Cossi, M.; Rega, N.; Scalmani, G.; Barone, V. Energies, Structures, and Electronic Properties of Molecules in Solution with the C-PCM Solvation Model. *J. Comput. Chem.* **2003**, *24*, 669–681. https://doi.org/10.1002/jcc.10189.

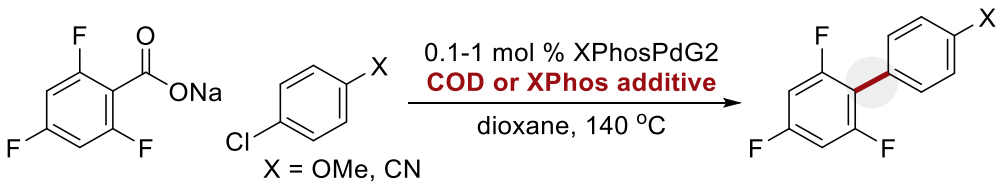

kinetics **eyring plot** **substituent effects** **DFT** **additive studies**

turnover limiting decarboxylation **additives improve catalyst performance**